Utrecht University

Master Thesis

Patchy Rough Colloids as Pickering Stabilizers

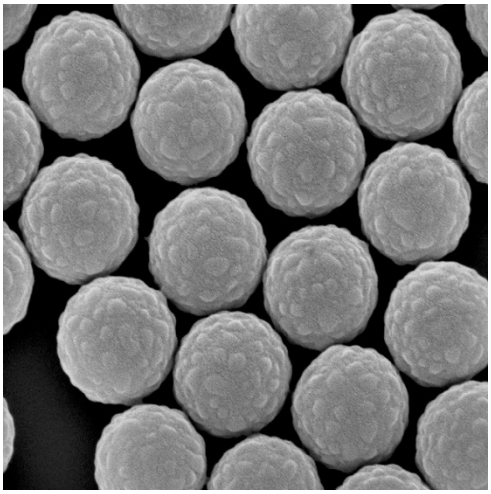
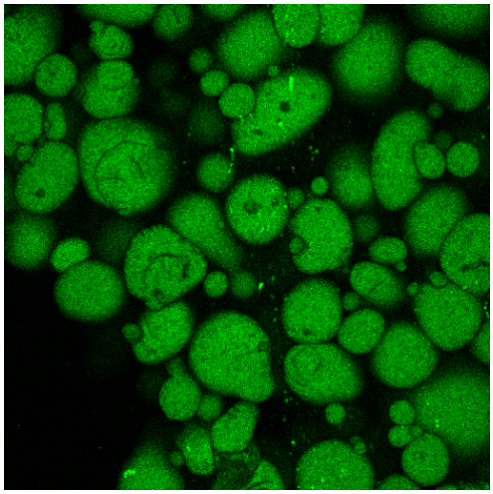

J. M. H. Weijgertze

Under supervision of:

M. Zanini

W. K. Kegel

Van 't Hoff Laboratory for Physical and Colloid Chemistry

Debye Institute for Nanomaterials Science

Utrecht University

January 2020

ABSTRACT

A Pickering emulsion is a dispersion of immiscible fluids stabilized by colloidal particles. Pickering stabilizers are typically considered to be perfectly smooth and chemically homogeneous. The use of rough and heterogeneous colloids is expected to fundamentally alter the properties of the formed emulsions. In particular, we investigate the role of surface structuring on emulsification and the catastrophic phase inversion of Pickering emulsions. To gain deeper fundamental insights into this topic, we fabricate in large amounts patchy rough particles comprising a polystyrene core with organosilicate asperities. Their roughness is characterized with AFM and an estimate of their composition can be obtained from their oxidative mass losses upon combustion. The chemical heterogeneity of the particle surfaces is estimated by measurements of the surface patchiness. The degree of surface heterogeneity is used to calculate the particles' contact angles at a water-decane interface, which are empirically measured by gel trapping technique. Systematic variations in emulsification shear rate, o/w ratio and particle type reveal the influence of particle heterogeneity on processing and formulation of emulsions. This work paves the way for a deeper understanding of the behavior of Pickering emulsions, where non-ideal, heterogeneous particles are present.

TABLE OF CONTENTS

1 INTRODUCTION

Emulsions are widely spread in many different fields of our daily life, such as in food,[1] cosmetics,[2] paints,[3] pharmaceutical products[4,5] and petroleum industries.[6] Conventionally, an emulsion is a mixture of two immiscible liquids, where one phase is present as droplets (the dispersed phase) in the other phase (continuous phase).[7] Surface active species stabilize the droplets and prevent emulsions from phase separation. Traditionally, surfactant molecules are used as emulsion stabilizers.[8] Since the pioneering work of Ramsden[9] and Pickering,[10] the potential of solid particles to stabilize emulsions has been recognized and exploited. Pickering emulsions can offer advantages over surfactant-stabilized emulsions, namely increasing the emulsion stability, providing more environmentally friendly processes and reducing the use of potentially toxic or skin-irritant chemical admixtures.[11]

In a Pickering emulsion, layers of solid particles on droplets create a steric barrier against coalescence.[12] Pickering stabilizers are typically considered as smooth and chemically homogeneous spheres.[5,13] However, the particles present in real systems often do not fulfil this premises. For instance, clay,[14,15] protein[11,16] and starch[17,18] particles have been extensively used as emulsion stabilizers especially in the food industry[18] despite the fact that they bear a wide variety of morphologies and have chemically heterogeneous compositions. Moreover, designing particles with a broad diversity of morphologies as Pickering stabilizers has gained interest in recent years. Such particles include Janus particles,[19] (Janus) sheets,[20,21] ellipsoids,[22] dumbbells[23] and rough particles.[24] Particle morphologies deviating from homogeneous spheres affect emulsification and give opportunities for different ways of efficient Pickering stabilization.[5,25]

In general, (Pickering) emulsions are a flexible material platform, where either oil-in-water (o/w) or water-in-oil (w/o) emulsion types can be accessed depending on emulsification conditions and processing.[26,27] In this work, the use of well-characterized patchy rough particles as Pickering stabilizers is investigated to better understand the effect of particle heterogeneity on emulsification. In particular, we focused on the role of surface structuring in phase inversion of emulsions. Phase inversion concerns the switch from an o/w to a w/o emulsion or vice versa.[26] It is relevant to many industrial processes, including the fabrication of cosmetic, food and pharmaceutical products, as well as crude oil recovery.[6,28] The obtained emulsion type is a crucial aspect for the final products. In fact, some applications such as oil-based skin creams[29] require w/o emulsions, while others such as mayonnaise require o/w emulsions.[30] Interestingly, in these applications, phase inversion is undesired since it would completely alter the product properties. Even more interestingly, in some cases e.g. in crude oil processing, phase inversion is deployed to recover the oil from emulsions.[31]

Herein, the o/w ratio and energy input during emulsification are systematically varied to gain more insight in the effect of surface heterogeneity on the emulsification and phase inversion of Pickering emulsions. In this regard, patchy rough particles comprising a polystyrene core with organosilicate asperities are fabricated. The roughness of these particles is characterized with atomic force microscopy (AFM) and the composition is obtained by thermogravimetric analysis (TGA). The equilibrium positions of the particles at a water-decane interface are estimated from their surface patchiness and compared to the contact angles measured with gel trapping technique (GTT) to underline the peculiar adsorption pathway of the non-ideal particles at the interface. In all our experiments, the colloids are initially dispersed in the aqueous phase, where they are charge stabilized. The considerations and conclusions reported here base on single-particle mechanisms.

2 THEORETICAL BACKGROUND

2.1 PICKERING EMULSIONS

When a liquid droplet enters in contact with a solid substrate, it can fully spread or partially wet the surface. In the latter case, a finite contact angle θ can be defined and it depends on the balance between the solid-vapor (γ_{SV}), solid-liquid (γ_{SL}) and liquid-vapor (γ_{LV}) surface tensions. These surface tensions find their origin in the molecular interactions and ultimately determine the wetting of a substrate. The concept of wetting in relation to surface tensions was formulated in 1805 by Thomas Young,[32] and is described by Young's law (see Figure 1a):

$$\cos\theta = \frac{\gamma_{SV} - \gamma_{SL}}{\gamma_{LV}} \quad (1)$$

This follows from the equilibrium of the forces (surface tensions) parallel to the solid surface.[33]

Analogously, the wetting of a particle adsorbed at an oil-water interface is described by (see Figure 1b):

$$\cos\theta = \frac{\gamma_{SO} - \gamma_{SW}}{\gamma_{WO}} \quad (2)$$

where γ_{SO}, γ_{SW} and γ_{WO} are the particle-oil, particle-water and water-oil interfacial tensions, and θ the contact angle of the particle measured through the water phase.[34]

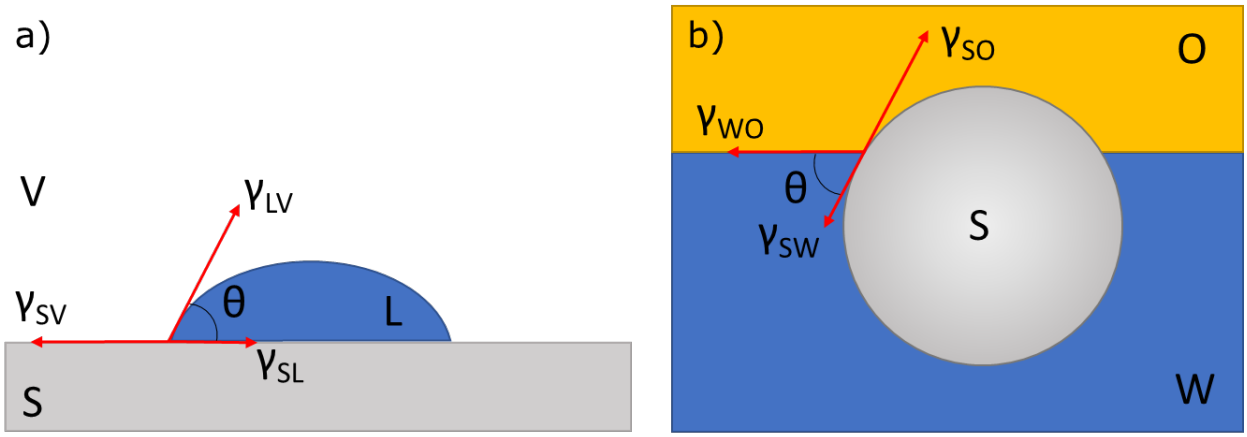

*Figure 1. Surface tension forces at the three-phase contact line of **(a)** a liquid drop on a solid surface and **(b)** a solid particle at an oil-water interface.*

When an oil and water are mixed in the presence of solid particles, the adsorption of these particles on the oil-water interface may result in the formation of an emulsion, where droplets of one phase remain dispersed in the other, continuous, phase.[35] The potential of particles to stabilize emulsions has been known since the work of Ramsden[9] and Pickering[10] in the early 1900s, hence the name Pickering emulsions for particle-stabilized emulsions (see Figure 2a). The particles used as emulsifiers are usually in the colloidal size range (nm-μm).[29]

By convention, the contact angle of particles at an oil-water interface is measured through the water phase. Then, hydrophilic particles have a contact angle θ < 90°, as they are immersed for the largest part in the water phase (Figure 2b). As a result, they impose a curvature of the interface such that they preferentially stabilize emulsions with oil droplets dispersed in the water continuous phase (o/w). Conversely, hydrophobic particles have contact angles θ > 90° and conventionally stabilize w/o emulsions (Figure 2c).

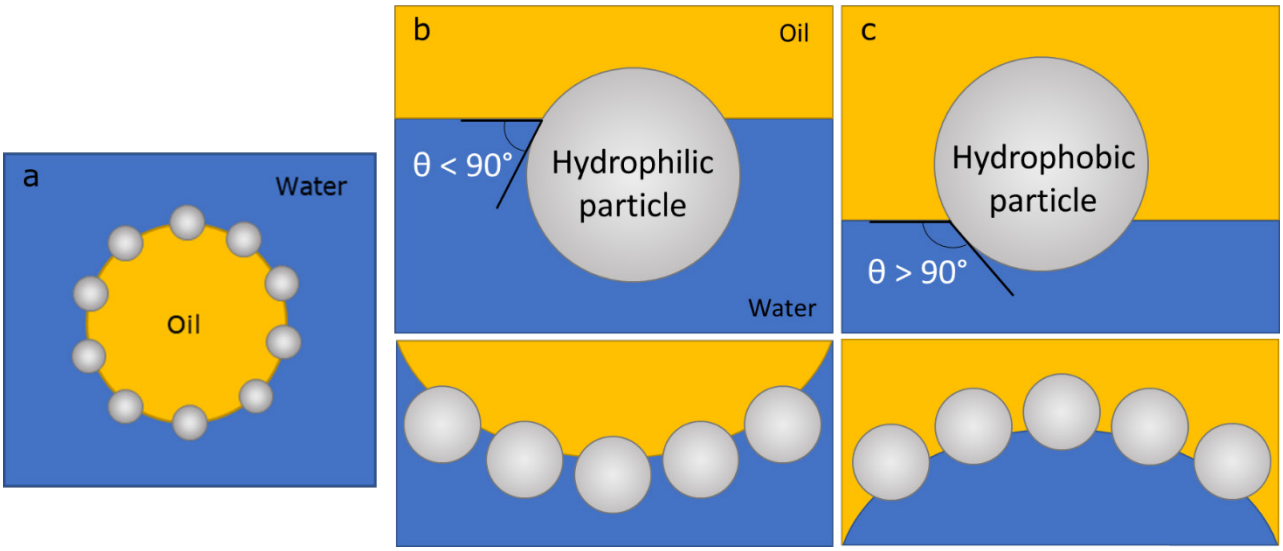

Figure 2. ***Particles adsorbed at an oil-water interface can stabilize Pickering emulsions. (a)*** *Schematic representation of an oil droplet in water stabilized by solid particles.* ***(b)*** *represents a hydrophilic particle with a contact angle θ < 90° that conventionally stabilizes o/w emulsions.* ***(c)*** *represents a hydrophobic particle with a contact angle θ > 90° that conventionally stabilizes w/o emulsions.*

The reason why particles can stabilize emulsions is their strong attachment to fluid interfaces. This can be understood considering the energies involved in adsorption (desorption) of a particle to (from) an oil-water interface. For regimes of Bond number $B_0 \ll 1$ (negligible gravity compared to interfacial tension)[35] and considering Figure 1b, the energy gain upon adsorption of a hydrophilic particle at the oil-water interface from the water reads:

$$\Delta G = -\gamma_{SW} 4\pi R^2 + \gamma_{SW} 2\pi R(R + Rcos\theta) + \gamma_{SO} 2\pi R(R - Rcos\theta) - \gamma_{WO} \pi R^2 sin^2\theta \qquad (3)$$

where R is the particle radius and θ the contact angle of the particle measured through the water phase. The first term corresponds to the lost surface energy of the particle completely dispersed in water, the second and third term to the creation of particle-water and particle-oil interfaces respectively, and the last term to the oil-water interface suppressed due to the presence of the particle at the interface. Thus, high values of γ_{WO} make it favorable for a particle to adsorb at the interface.[8] Rearranging Eq. (3) using Young's law gives the energy for the attachment of a particle to an oil-water interface:

$$\Delta G = -\pi R^2 \gamma_{WO}(1 - |\cos\theta|) \qquad (4)$$

Evaluating this equation using γ_{WO} = 51 mN/m for a water-decane interface[36] and a particle radius R of 400 nm gives a maximal adsorption energy (θ=90°) of $-6 \cdot 10^6$ kT at 20°C. This value applies for the emulsifiers used in this work. The attachment energy is significantly greater than the thermal energy also for particles down to ~10 nm and for contact angles between 30° and 150°.[29,35] Because of this incredibly strong attachment, particles are considered as irreversibly trapped at the interface.[35] Therefore, particle films on emulsion droplets form a steric barrier against coalescence and are responsible for emulsion stabilization.[12] It is important to realize that Pickering systems are inherently metastable; they are stable only due to the large (~infinite) kinetic barrier for particle desorption.[37] Emulsions will eventually completely phase separate towards thermodynamic equilibrium.[6] Additional stabilization of Pickering emulsions may arise from the formation of a three-dimensional particle network in the continuous phase (bulk stabilization).[12,38]

2.2 WETTING OF ROUGH AND HETEROGENEOUS (PARTICLE) SURFACES

In the previous section, only the simplest case of wetting of ideal homogeneous surfaces is discussed. However, in real systems, most surfaces are inhomogeneous, namely contaminated, rough, and/or chemically heterogeneous.[32] For such surfaces, some extensions to the general Young's law are formulated.

For the wetting of heterogeneous surfaces, where distinct areas of the composite have different wettability, Cassie's law[39] is applied. The free energy change per unit area caused by a liquid spreading over a solid surface consisting of two components with fractional areas σ_1 and σ_2 is given by:

$$E = \sigma_1 * (\gamma_{S_1V} - \gamma_{S_1L}) + \sigma_2 * (\gamma_{S_2V} - \gamma_{S_2L}) \quad (5)$$

with surface tensions as defined in Figure 1a but with the subscripts 1 and 2 referring to the different solid components. The contact angle θ for the composite surface is:

$$\cos\theta = \frac{E}{\gamma_{LV}} \quad (6)$$

Filling in the energy E in Eq. (6) and substituting Young's law for the contact angles θ_1 and θ_2 of the separate solid components gives for the wetting of a heterogeneous solid:

$$\cos\theta = \sigma_1 \cos\theta_1 + \sigma_2 \cos\theta_2 \quad (7)$$

Equation (7) is known as Cassie's law. In Figure 3a, the heterogeneous wetting according to Cassie's law is depicted. The orange and the grey area are the two chemical components of the surface.

Cassie's law also applies to the special case of a rough surface. Then, the orange cavities in Figure 3a are treated as air pockets instead of solid. Assuming complete dewetting between liquid and vapor (θ_2 = 180° and $\sigma_2 = \sigma_{LV}$), Cassie's law transforms into the Cassie-Baxter equation[33] for heterogeneous wetting of a rough surface:

$$\cos\theta^* = (1 - \sigma_{LV})\cos\theta_0 - \sigma_{LV} \quad (8)$$

with θ^* the apparent contact angle and θ_0 the equilibrium contact angle on the solid surface. As opposed to heterogeneous wetting, a rough surface can also be wetted homogeneously. This behavior is described by the Wenzel state (Figure 3b). Here, the liquid penetrates into the cavities between the asperities on the rough surface. In this case, the apparent contact angle on the rough surface is given by the Wenzel equation:

$$\cos\theta^* = r\cos\theta_0 \quad (9)$$

where θ_0 is again the equilibrium contact angle on the smooth solid surface, and r is the roughness factor equal to the ratio of the complete surface area to its flat projection.

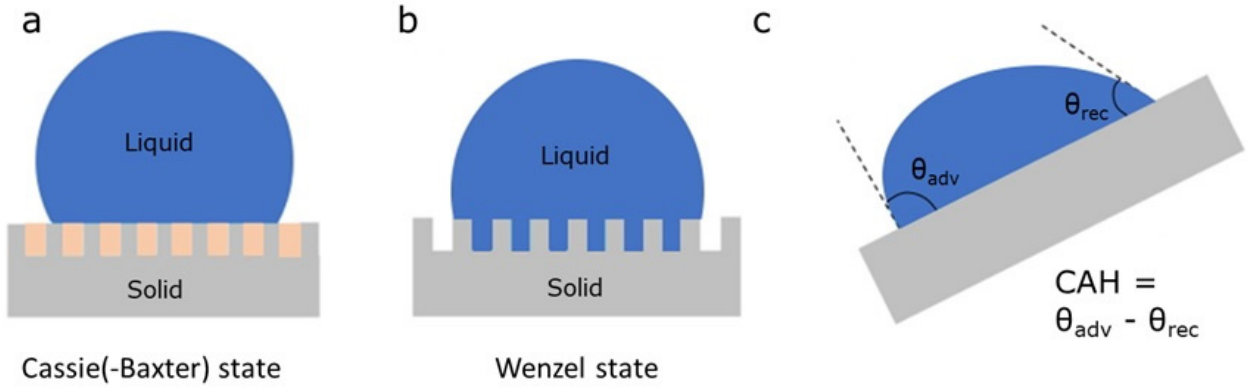

Figure 3. ***Schematic drawing of wetting of rough and heterogeneous surfaces. (a)*** *Cassie state for the wetting of a solid composed of two chemical components (grey and orange) or Cassie-Baxter state when the orange cavities are filled with air.* ***(b)*** *Wenzel state for homogeneous wetting of a rough surface by a liquid.* ***(c)*** *Contact angle hysteresis (CAH) can be measured from a liquid drop on a tilted substrate. Adapted from ref.* [33]

In Eq. (5)–(9), it is assumed that the liquid drop reaches its equilibrium contact angle independent of the way the droplet is deposited on the substrate.[32] On real surfaces however, pinning of the contact line on surface heterogeneities or contaminations often leads to a range of attainable contact angles, depending on how the fluid approaches the substrate. For example, when aqueous solution is added to an existing water droplet on a solid substrate, the droplet edges initially pin on the surface, resulting in an effectively larger contact angle, called the advancing contact angle θ_{adv}. Likewise, the receding contact angle θ_{rec} is observed when the volume of an existing droplet is decreased. Advancing and receding contact angles can be measured on a tilted solid substrate (Figure 3c). The difference in the advancing and receding contact angle, $\theta_{adv} - \theta_{rec}$, is known as the contact angle hysteresis.[33]

The here described wetting effects also apply to wetting of colloids at oil-water interfaces. In the case of rough colloids, it was suggested that their efficiency as Pickering stabilizers is optimal when their wetting is still in the Wenzel regime.[40] It was found that both the stability[40] of Pickering emulsions and particle adsorption efficiency[41] initially increase with the roughness, and immediately drop beyond a given roughness level. This non-monotonic trend was explained as a transition from the Wenzel to the Cassie-Baxter wetting regime. In the latter scenario, the surface exposed to the apolar phase is not homogeneously wet by oil, yet has imbibed water in the cavities between the particle's asperities.

In addition, contact line pinning on rough particle surfaces has been proved to have pronounced effects on the behavior of rough particles at interfaces and on emulsification. As mentioned above for macroscopic surfaces, the pinning of droplet edges (or, more general, contact lines) on the solid gives rise to contact angle hysteresis. Similarly, the asperities of a rough particle approaching the interface from e.g. the water phase can strongly pin the contact line and effectively arrest adsorption in metastable positions. This means that the particle cannot reach its equilibrium position at the interface and appears more hydrophilic than it would be anticipated from its mere surface chemistry. When the same particle approaches the interface from the oil, the mirrored situation can happen, where the particle is trapped in a position in which it remains more immersed in the oil. The difference between the effective contact angles of these two configurations is the contact angle hysteresis. This phenomenon has deep consequences in the preparation of emulsions, since the same particles can stabilize both o/w and w/o depending on the phase in which they are initially dispersed.[24]

In addition to the modification of the adsorption-kinetic pathway, contact line pinning on rough or heterogeneous particle surfaces distorts the liquid interface surrounding the colloid (see Figure 4a).[42] Interfacial deformations originate to satisfy Young's law all along the perimeter of the particle.[43] In order to rationalize the interfacial deformations around colloidal particles trapped at liquid interfaces, the height of the contact line h can be decomposed into multipoles using a common multipole expansion:[42]

$$h(r,\varphi) = \sum_{m}^{\infty} H_m \cos\left(m\left(\varphi - \varphi_{m,0}\right)\right) \tag{10}$$

where r and φ are cylindrical coordinates, $\varphi_{m,0}$ are constants that follow from boundary conditions, H_m are expansion coefficients in which r is included and m is the expansion order. The general idea of a multipole expansion is the description of features with progressively finer angular dependence for each higher multipole order. For instance, electric potential is commonly described in terms of multipoles, with a single charge being a monopole and two opposite charges separated at a small distance being a dipole.[44] For rough or heterogeneous colloidal particles, the first non-zero term in the multipole expansion is the quadrupole.[42] Figure 4b clearly shows the quadrupolar symmetry of the interfacial deformations around a rough particle. Distortions of the meniscus give rise to capillary interactions,[45] i.e. interactions between particles mediated by fluid interfaces.[46] Particles attract each other only when their overlapping menisci are of like sign (e.g. both concave or convex). Conversely, they repel.

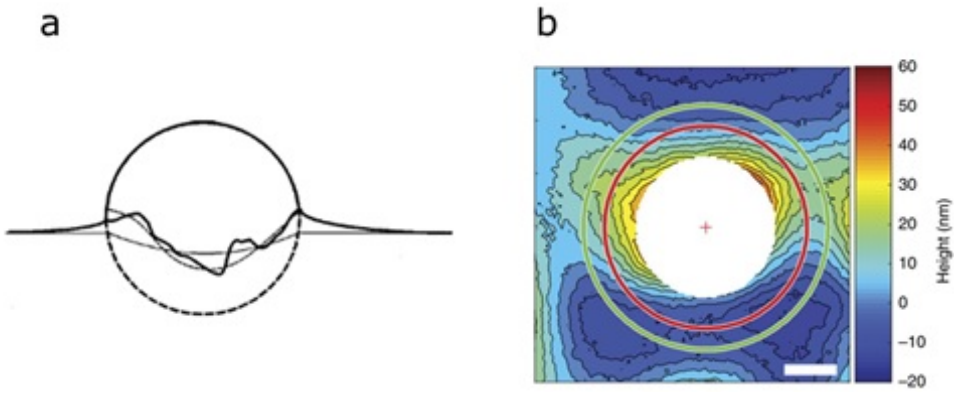

Figure 4. ***Interfacial deformations around rough particles. (a)*** *Schematic description of an undulated contact line on a rough or heterogeneous particle. Pinning of the contact line on surface heterogeneities causes distortion of the surrounding interface.* ***(b)*** *Height contour plot of the interface around a rough particle showing the quadrupolar interface deformation. Reprinted from (a) ref.*[42] *and (b) ref.*[24]

Interestingly, the quadrupolar capillary interactions affect the rheology of interfaces laden with rough or heterogeneous particles. Particles form percolating networks under influence of their capillary interactions, which can enhance the elastic response of the interface, as well as lead to higher effective interfacial viscosity compared to interfaces with smooth and homogeneous particles.[47] It was proposed that the increased elasticity of interfaces laden with rough carbon black particles promotes Pickering emulsion stability by preventing droplet deformation and coalescence.[48] The link between interfacial rheology and stability of Pickering systems has been additionally expended to foams.[49]

2.3 Emulsion phase inversion

In this work, emulsification and in particular the (catastrophic) phase inversion of Pickering emulsions with patchy rough particles is investigated. Traditionally, two types of phase inversion are distinguished, i.e. the transitional and catastrophic phase inversion. The former occurs via a change in particle wettability,[31] which can be induced by changing temperature, oil type, pH or salinity.[12,50] Catastrophic phase inversion is induced by a change in the volume fraction of the dispersed phase (see Figure 5).

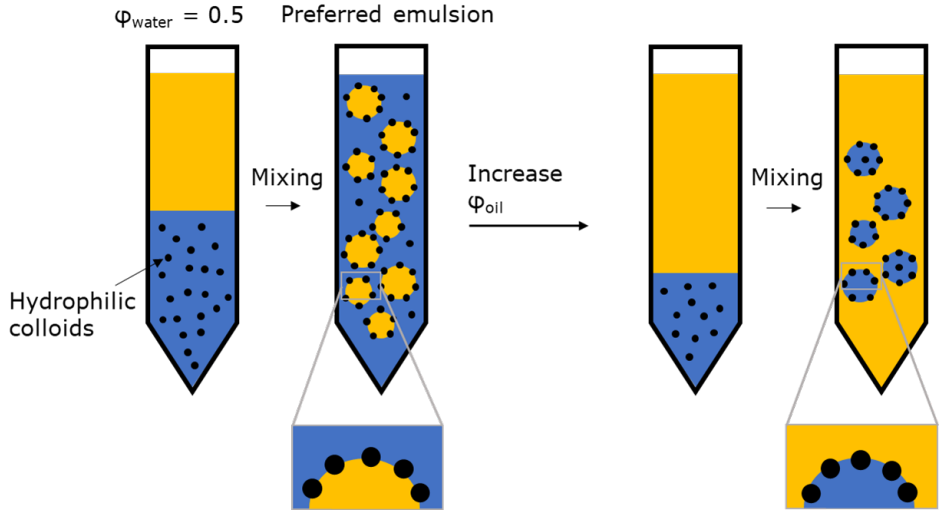

Figure 5. ***Catastrophic phase inversion.*** *By increasing the volume fraction of oil (φ_{oil}), an o/w emulsion can be inverted to a w/o emulsion (and vice versa). Hydrophilic colloids preferentially stabilize an o/w emulsion, which is of Bancroft type (i.e. the phase in which the emulsifier is stably dispersed constitutes the continuous phase).*[51] *The inverted emulsion (w/o) is of anti-Bancroft type.*

At sufficiently large volume fractions of dispersed phase the rate of drop coalescence is higher than the rate of drop breakup, eventually leading to phase inversion.[26] Nearby the inversion point, multiple emulsions are often observed.[52] These form by inclusion of continuous phase into drops of the dispersed phase as they coalesce together.[53]

The onset of catastrophic phase inversion can depend on the particle wettability[53] and on the added volume of dispersed phase.[26] Early theories base on the exceeding of a critical packing fraction of droplets of dispersed phase (0.64–0.74 for random to closed packing of monodisperse spheres) to explain the phase inversion.[54] Further analysis based on a pure thermodynamic model showed that phase inversion should occur at any slight deviation from $\varphi_{water} = 0.5$.[55] For instance, an o/w emulsion should invert to w/o as soon as φ_{water} becomes smaller than 0.5. This is a result of the more favorable energy of formation of new oil-water interface when the phase with the largest volume fraction constitutes the continuous phase. Curvature energies are only relevant at $\varphi_{water} = 0.5$; i.e. at equal volume fraction of the phases. For this peculiar case, the particle wettability determines whether o/w or w/o is the preferred emulsion type. Interestingly, experimental investigations show that catastrophic phase inversion often happens at volume fractions of dispersed phase of 0.6–0.7.[56,57] Deviations from the thermodynamic model can originate from the assumptions made in the model, which include: (1) very fast particle adsorption, (2) no particle desorption, (3) no contact angle hysteresis for the particle wetting, (4) treatment of particles as monodisperse spheres and (5) the lack of kinetic barriers preventing the emulsion to reach its minimal free energy without being phase separated. Thus, kinetic factors are not taken into account. The latter could explain why the phase inversion occurs at volume fractions higher than the thermodynamic estimations. Examples of such kinetic effects are the faster hydrodynamic transport of particles in the continuous phase than inside droplets (making the adsorption of particles from the continuous phase easier) and the presence of barriers against particle adsorption and contact angle equilibration.

Remarkably, for particles having a large contact angle hysteresis, phase inversion can be triggered upon mechanical input.[58] This refers to the inversion of an emulsion upon increasing energy input during emulsification. In this peculiar system, at low energy input, a mildly hydrophobic particle (initially dispersed in the water phase) adsorbs in a metastable position at the oil-water interface remaining more immersed in the water phase (see Figure 6). In this configuration, contact line pinning arrests the particle motion through the interface imposing an effective contact angle and therefore imparting a preferential curvature of the liquid interface. In this case, o/w emulsions are formed. At sufficiently high emulsification energies, the contact line can relax and jump over the particle pinning points. The kinetic energy barrier that prevented the particle from reaching its equilibrium position is overcome and the o/w emulsion inverts to a w/o emulsion. The mirrored situation is also possible and it has been validated.[58]

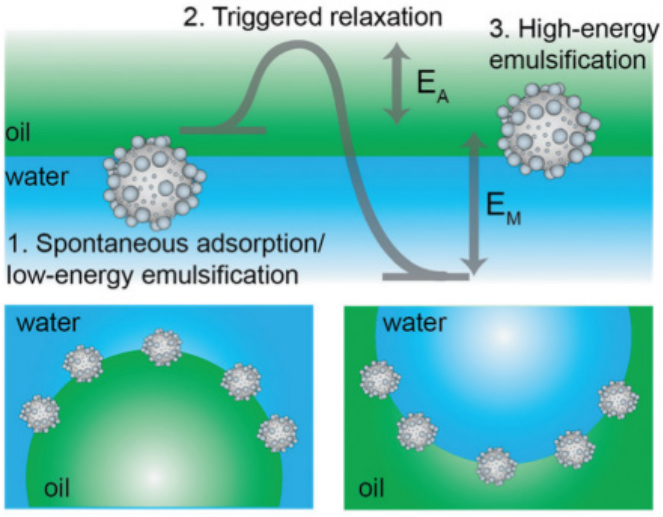

Figure 6. Mechanical phase inversion from an o/w to a w/o Pickering emulsion. Reprinted from ref.[58]

3 MATERIALS AND METHODS

3.1 MATERIALS

Chemical	Abbreviation	Supplier
Silica gel, high-purity grade: Davisil Grade 633		Sigma-Aldrich
Aluminum oxide, Puriss., ≥98% Al2O3 basis		Honeywell Fluka
Styrene, ≥99%, contains 4-tert-butylcatechol as stabilizer		Sigma-Aldrich
4-Styrenesulfonic acid sodium salt hydrate	NaSS	Sigma-Aldrich
2,2'-Azobis(2-methylpropionitrile), 98%	AIBN	Sigma-Aldrich
Methanol absolute HPLC	MeOH	Biosolve Chimie
Divinylbenzene, technical grade 80%	DVB	Sigma-Aldrich
Methacryloxyethyl thiocarbamoyl rhodamine B	PolyFluor®570	Polysciences
Ammonium hydroxide, for analysis, 28-30 wt% in water	NH_3	Acros Organics
3-(Trimethoxysilyl)propyl methacrylate, ≥97%	TPM	Sigma-Aldrich
Gellan Gum, powder	Gellan	Alfa Aesar
Ethanol absolute	EtOH	VWR Chemicals
Norland optical adhesive 81	UV glue	Norland Products
Pyrromethene, BODIPY™ 493/503	BODIPY	Invitrogen™
Potassium chloride, ≥99%	KCl	Acros Organics
n-Decane, ≥99%		Carl Roth GmbH
Hydrochloric acid, for analysis, fuming, 37% in water	HCl	Acros Organics

Styrene was purified through a column packed with silica gel (1/2 column height) and aluminum oxide powder (1/2 column height). The other chemicals were used as received. Water used in all experiments was purified by filtration through Millipore filters (18.2 MΩ·cm at 25 °C).

3.2 POLYSTYRENE CORE PARTICLE FABRICATION

Cross-linked sulfonated polystyrene (PS) particles were fabricated via dispersion polymerization.[59] Since the reaction medium is a good solvent for the monomer, the mixture is initially homogeneous.[60] The formation and precipitation of polymer particles creates a dispersion.

For the synthesis, 5 mL styrene, 90 mg NaSS and 90 mg AIBN were dissolved in 10 mL water and 40 mL MeOH in a 100 mL round-bottomed flask. The size of the polymer particles can be tuned by varying the MeOH/water ratio. With a lower MeOH/water ratio, the growing chains phase separate at earlier stages, thus shorter styrene condensates can be stabilized, yielding smaller sphere sizes. The flask was sealed with a rubber septum and flushed with N_2 (g) for 30 minutes under magnetic stirring at 200 rpm. Next, the flask was immersed in a pre-heated oil bath (65°C) and the mixture was stirred magnetically at 200 rpm. After 5 hours, a pre-heated (50°C) mixture of 0.5 mL styrene, 165 µL DVB, 90 mg AIBN and 1 mg PolyFluor®570 in 5 mL MeOH was added to cross-link the polymer particles and equip them with a fluorescent label. The polymerization was carried out for 24 hours.

The resulting polystyrene particles were washed three times in MeOH/water by centrifugation at 3270 × g (Beckman Coulter Allegra® X-12R). Washing in a MeOH/water mixture rather than in only water facilitated sedimentation and redispersion of the particles. If necessary, redispersion was promoted by mechanical agitation and sonication. Rotary evaporation was used to remove

MeOH and the PS particles were further processed in water. The final particle concentration of the PS core dispersions was 3.5–4.0 wt%.

3.3 Fabrication of patchy rough colloids

In order to obtain sufficient amounts of particles to extensively study their emulsification behavior, the synthesis was scaled to yield nearly a gram of patchy rough (or raspberry-like) particles. Taking inspiration from Stefano Sacanna's work,[61] it was chosen to heteronucleate and polymerize the organosilicate TPM on PS cores. To do so, a volume of 20-30 mL PS core dispersion was added to a 2L Teflon bottle containing 974 mL water and 52 mL NH_3 (pH 11.5) such that the PS particle concentration in the final reaction volume was circa $3 \cdot 10^{12}$ particles/mL. TPM was added in the range of 0.17–0.32 vol% with respect to the total reaction volume to obtain different degrees of particle roughness and composition. The bottle was agitated on a tumbling table (IKA® KS 260 basic) for 90 minutes at 150 rpm. This allowed the TPM to undergo a sol-gel process[62] and to heteronucleate on PS spheres. Thereafter, the reaction mixture was transferred to a 2L round-bottomed flask and 240 mg of AIBN (initiator)[63] was added. During this step, 280 µL of 1 mg/mL BODIPY in DMSO can be added to label the asperities with a green fluorescent marker. The flask was flushed with N_2 (g) for 15 minutes and sealed before being immersed in an oil bath (80°C). The TPM was polymerized on the PS cores under magnetic stirring at 200 rpm for 2 hours. The fabricated patchy rough particles were washed three times by centrifugation at 10,000 × g (Beckman Coulter Avanti J-26 XP, rotor JLA-16.250) and redispersion in water.

3.4 Scanning Electron Microscopy

PS particle size distributions were determined from SEM images (Scanning Electron Microscopy, Phenom ProX). The surface topography of the fabricated patchy rough particles was visualized with SEM (XL30S FEG, FEI). SEM samples were prepared by drying a suspension droplet on a hydrophilized Si wafer (Sil'Tronics 1–20 Ωcm, P-doped; glow-discharged with a Cressington Carbon Coater 208C and Power unit 208APU). The samples were sputter coated with a few nm of Pt to prevent charging (Cressington Sputtercoater 208HR). All SEM samples reported in this work were prepared in the same manner.

3.5 Zeta potential

Zeta potential measurements of ~0.03 wt% PS particle suspensions in 10 mM KCl were conducted with a Malvern Zetasizer Nano ZS in a disposable cuvette (polystyrene, 4 mL, SARSTEDT AG & Co. KG). The Smoluchowski model was applied to extract the zeta potential.

3.6 AFM roughness characterization

The surface roughness of the produced particles was measured by scanning a particle monolayer with Atomic Force Microscopy (AFM, JPK Nanowizard II). AFM samples were prepared by convective assembly[64] of particles on a hydrophilized glass slide (VWR cover glass 22x22 nm 1.5 nm thickness, glow-discharged with a Cressington Carbon Coater 208C and Power unit 208APU). The particle surface was probed with an Olympus AC160TS-R3 silicon cantilever with a resistivity of 0.01–0.02 Ωcm, a spring constant of 26 N/m and a resonance frequency of 300 kHz at room temperature and ambient relative humidity.

The resulting AFM height profiles were analyzed to characterize the particle roughness. In the field of surface sciences, a common parameter to describe the amplitude of the roughness is the

RMS (root-mean-square) roughness.[65] For particles with similar size and surface topography, the RMS roughness is a suitable roughness descriptor.[66] Since the fabricated patchy rough particles satisfy these criteria, RMS roughness was selected as the appropriate parameter to describe the particle roughness.

From the resulting AFM height profiles, the RMS roughness can be extracted. This was done using a least-square based algorithm[66] that decouples the signal of interest from the underlying curvature. The RMS roughness can then be calculated using the following standard definition for root-mean-squared deviations:

$$RMS\ roughness = \sqrt{\frac{1}{n}\sum_{i=1}^{n} y_i^2} \tag{11}$$

This means that the surface is sampled over n points with each a corresponding height y normal to the fitted sphere. The calculated RMS was considered reliable and was accepted when the fitted particle radius was within 10% of average core particle radius independently determined by SEM. In this way, the preserved diameters capture most of the diameters in the histograms presented in Figure 8 in section 4.1.1.

3.7 THERMOGRAVIMETRIC ANALYSIS (TGA)

To estimate the composition of the patchy rough particles, a thermogravimetric analysis was performed. For each measurement, 0.5–1.5 mL of particle dispersion at 2–4 wt% was dried in a porcelain dish (Incinerating dishes porcelain 33d/3, IDL GmbH) in an oven. Thermogravimetric analysis was conducted using a Nabertherm P330 furnace. The samples were heated to 650 °C at a heating rate of 7 °C/min and kept 30 min at 650°C before cooling down to room temperature.

The mass of different patchy rough particles before and after calcination was determined on an analytical balance. From these values, the composition of the particles expressed as mass% of TPM could be calculated taking into account the difference in oxidative mass losses upon combustion of PS and TPM. In Appendix B, the calculation is explained in detail.

3.8 SURFACE PATCHINESS ESTIMATION

Since the patchy rough particles are composed of PS cores with TPM asperities grown on it, the surface of the particles is chemically heterogeneous. As a quantification of the partition between PS and TPM surface area, the surface patchiness was estimated. In this work, the surface patchiness is defined as the fraction of TPM patches on the total surface.

SEM images (SEM XL30S FEG, FEI) were used for surface patchiness analysis. From the SEM images, the average asperity size and the average number of asperities per particle were measured (representative images can be found in Appendix C). For a 2D surface patchiness estimate, the area of the TPM asperities was approximated as their projected area. Alternatively, for a 3D estimate the TPM asperities were approximated as spherical caps with an average base radius calculated from the SEM asperity size and an average height extracted from AFM height maps.

3.9 CONTACT ANGLE MEASUREMENTS

To study the adsorption and wetting of the fabricated particles, the particle contact angles at a water-decane interface were measured using Gel Trapping Technique (GTT).[67]

The workflow for GTT is schematically represented in Figure 7. First a 2 wt% Gellan solution in water was prepared by stirring the mixture for 2 hours at 80°C. The Gellan solution was poured

in a 35 mm Petri dish containing n-decane inside an oven (Memmert Model 100-800) at 70 °C. Particle dispersions of 0.1–2 wt% in water/EtOH 50/50 v/v were spread on the interface by pipetting two times 5 µL at the Gellan/water-decane interface. The addition of EtOH to the particles dispersions favors the spreading of particles at the interface driven by a Marangoni flow.[68]

To reliably determine contact angles with this technique, it is important that Gellan addition to water does not significantly alter the adsorption of the particles at the interface. As indication, the contact angle of a water drop under decane on hydrophobized glass is invariant to the Gellan concentration in the aqueous phase.[69]

After spreading the particles, the samples were slowly cooled down to room temperature, whereby the aqueous phase jellified such that the particles were immobilized at the interface. Interface replicas were obtained by replacing the n-decane with UV glue and curing the glue by UV illumination. In this manner, the particles are partially embedded in the UV glue, preserving their positions at the interface. The replicas were imaged with SEM (Phenom ProX). Details on the calculation of the contact angles from SEM images can be found in Appendix D.

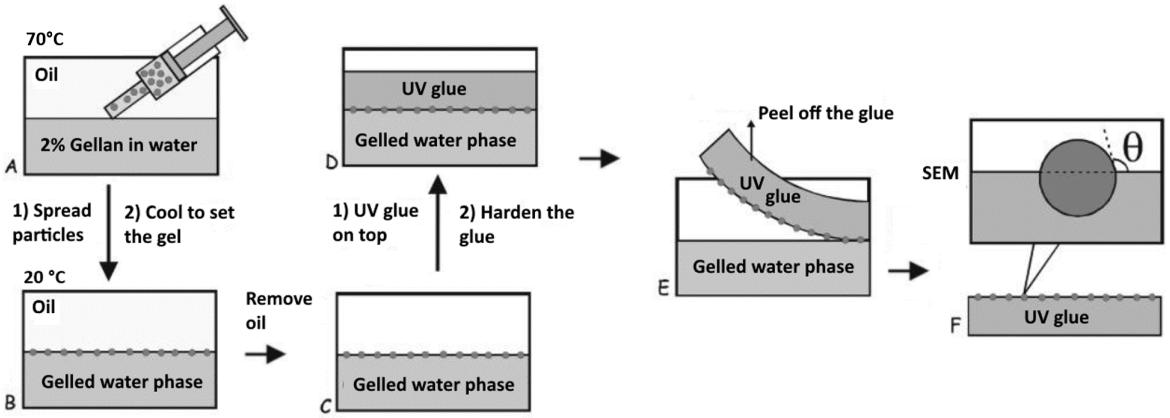

Figure 7. Workflow for Gel Trapping Technique. Adapted from ref. [67]

3.10 EMULSION PREPARATION

To investigate the effect of the use heterogeneous particles compared to homogeneous particles on emulsification and phase inversion, emulsions were prepared with different o/w ratios at different shear rates.

Emulsions with the patchy rough particles were produced according to the formulations given in Table 1. As a reference, bear PS cores and all-TPM particles were used as emulsifiers. The synthesis and characterization of all-TPM particles is described in Appendix A. The water phase of the emulsions was prepared by adding 0.1 M KCl to 2–3 wt% particle dispersions in water to yield water phases at the weight percentages given in Table 1. 10^{-3} mg/mL BODIPY was added in the n-decane oil phase to obtain sufficient optical contrast between the oil and water phase and directly visualize the formed emulsion type via fluorescence microscopy.

Table 1. Emulsion formulations. In the oil phase, BODIPY is added. The aqueous phase contains 0.1M KCl and the particles.

Water fraction (φ_{water} vol-ratio)	Oil phase (mL)	Water phase (mL)	Wt% particles in water phase
0.3	4.2	1.8	1
0.5	3	3	1
0.7	1.8	4.2	0.43

The concentration of particles in the aqueous phase was 0.43 wt% for φ_{water} = 0.7 to ensure that the particle concentration in the total emulsion volume was the same for φ_{water} =0.3 and 0.7. The pH of the emulsions was adjusted to 5.5-6.5 (monitored by a HANNA Instruments pH 210 pH meter with a Mettler Toledo InLab® Micro electrode) by adding a maximum of 120 µL 0.2 M HCl and a proportional amount of oil phase. Similar ionic strength and pH of the emulsions are of importance because variation in these quantities may induce transitional phase inversion linked to (de)ionization of PS sulfate and TPM silanol surface groups.[70]

The emulsification was performed with an IKA® T25 digital Ultra-Turrax homogenizer at 8,000 rpm, 14,000 rpm or 20,000 rpm for 1 minute.

3.11 EMULSION CHARACTERIZATION

The emulsions were imaged and characterized by bright field and fluorescence microscopy within a day after their preparation. Microscopy samples were prepared by carefully pipetting emulsion droplets in a custom-made cell consisting of two glass slides (Thermo scientific Menzel Gläzer microscope slide 76x26mm) glued on top of each other, where a hole of 1.5 cm in diameter had been cut out. The cell was sealed with a cover glass (VWR cover slip 22x22 mm, 1.5 nm thick).

The obtained emulsion type (o/w or w/o) was observed with a Nikon Eclipse TE2000-U equipped with a Nikon D-Eclipse C1 Laser scanning confocal microscope system. A 488 nm Ar laser was used for excitation of the BODIPY dye in the oil phase.

Bright field images were collected with either a Nikon Eclipse Ti-E microscope with a Hamamatsu Digital Camera C11440 ORCA-flash 4.0 (2048x2044 px images) or a Nikon Eclipse Ti-U microscope with a Imaging Source DFK 33UX249 (1920x1200 px images).

4 Results and Discussion

4.1 Fabrication of PS/TPM patchy rough colloids

4.1.1 Polystyrene core particles

Dispersion polymerization of styrene and 4-styrene sulfonic acid in a water/MeOH reaction medium yielded the PS particles shown in Figure 8. The synthesis leads to monodisperse colloids and to reproducible particle size. Slight deviations in the reaction conditions might cause some variation in particle size between different batches. Three batches of PS particles (PS-0, PS-I and PS-II) were produced. These particles serve as cores for the fabrication of patchy rough particles. The sulfate groups on PS originate from 4-styrene sulfonic acid and render the surface sufficiently negatively charged to maintain colloidal stability during the patchy rough particle synthesis.[71] Average zeta potentials are in the range of -45 to -65 mV (see zeta potential distributions in Appendix E).

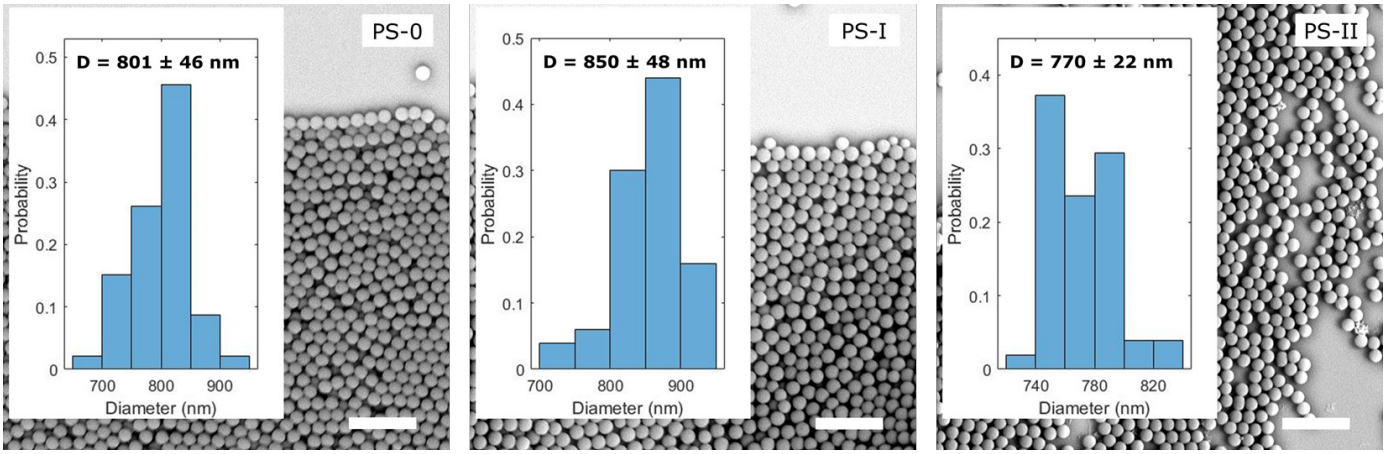

Figure 8. SEM images of polystyrene (PS) particles and size distributions determined from the images. Scalebars: 4 µm.

4.1.2 Patchy rough colloids

Particles of various morphologies can be produced by heteronucleation and polymerization of TPM on pre-fabricated sulfonated PS particles. The formation of bumpy asperities of TPM on PS relies on the finite wetting between the two materials. The size and number of asperities formed on the PS particles depends on both the concentration of TPM monomer and the pH set during the synthesis. Increasing the concentration of TPM monomer results in larger lobes, while increasing the pH produces smaller and more numerous asperities (Figure 9a).

To obtain patchy rough particles, the synthesis conditions were finely adjusted such that 'berry-covered' surfaces were formed. In literature, particles with such a morphology are also commonly referred to as raspberry-like particles.[66,72] Figure 9b schematically shows the path followed for the fabrication of patchy rough particles. In the first stage, TPM hydrolyses and condensates via its silanol group[62] heteronucleating on the surface of the PS cores. Radical polymerization of the methacrylate moiety creates solid raspberry-like particles. The procedure presented in this work yielded up to a gram of patchy rough colloids per synthesis, which is an adequate amount to extensively study the emulsification of the particles.

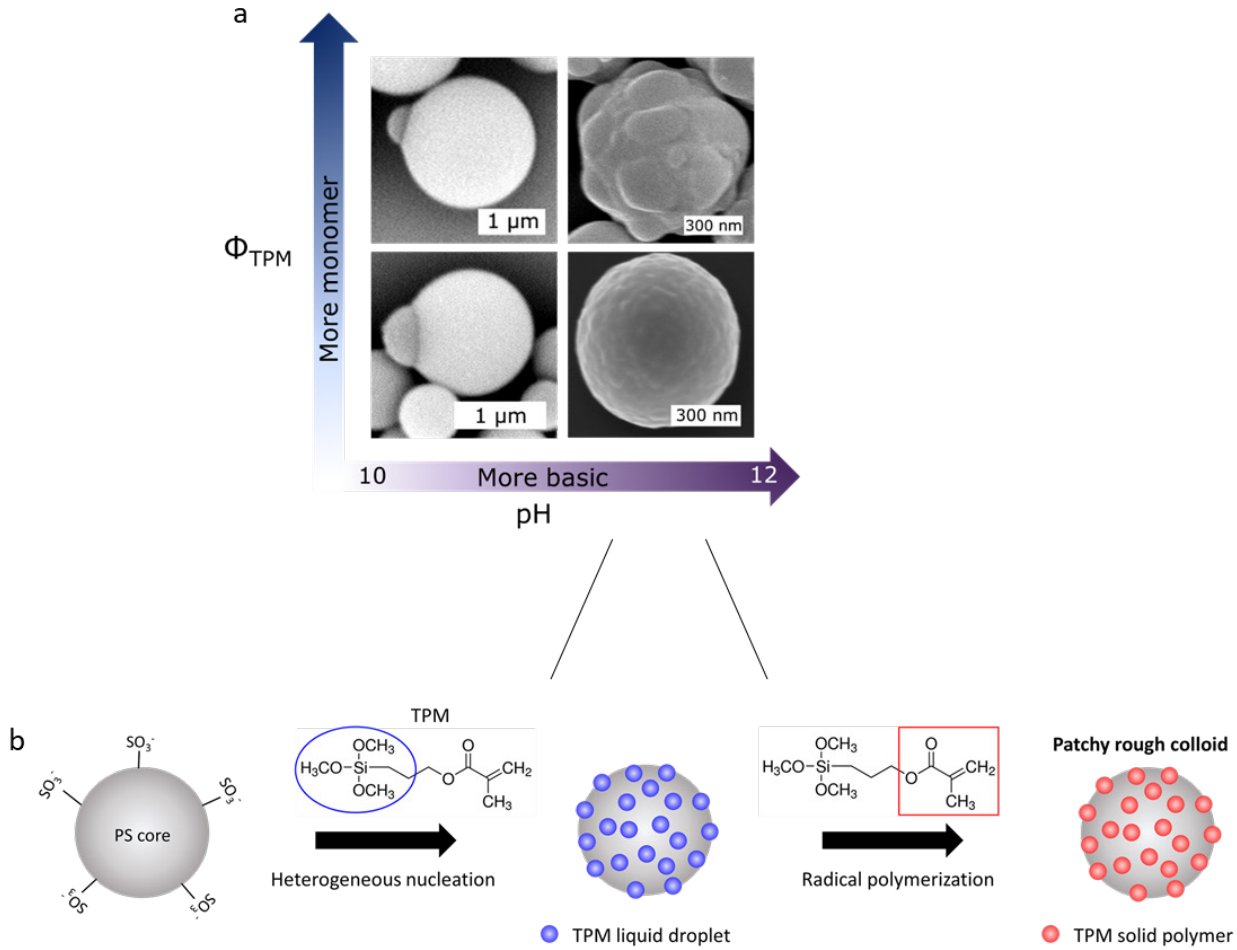

Figure 9. ***PS/TPM particle fabrication. (a)*** *Dependence of the surface morphology on volume fraction (ϕ) TPM and pH.* ***(b)*** *Schematic of the patchy rough colloid synthesis.*

Particles with different degrees of roughness and composition were fabricated by varying the volume fraction of TPM at constant pH (pH = 11.5). The increased size of TPM condensates by increasing TPM volume fraction at constant pH was verified for homogeneous nucleation of TPM (see Appendix A). Table 2 lists the fabricated particles in order of increasing roughness with the corresponding PS core particle and vol% TPM in the reaction mixture. The particle names refer to 'Raspberry' (RB) and their average RMS roughness in nm (as reported in section 4.2).

Table 2. Fabricated patchy rough particles in this work. pH = 11.5.

Patchy rough particle	PS core	Vol% TPM
RB-4.1	PS-0	0.17
RB-4.6	PS-I	0.20
RB-7.5	PS-II	0.22
RB-16	PS-I	0.25
RB-20	PS-0	0.32

4.2 Roughness and chemical composition

The surface topography of the fabricated patchy rough particles is imaged and characterized by both SEM and AFM, as shown in Figure 10.

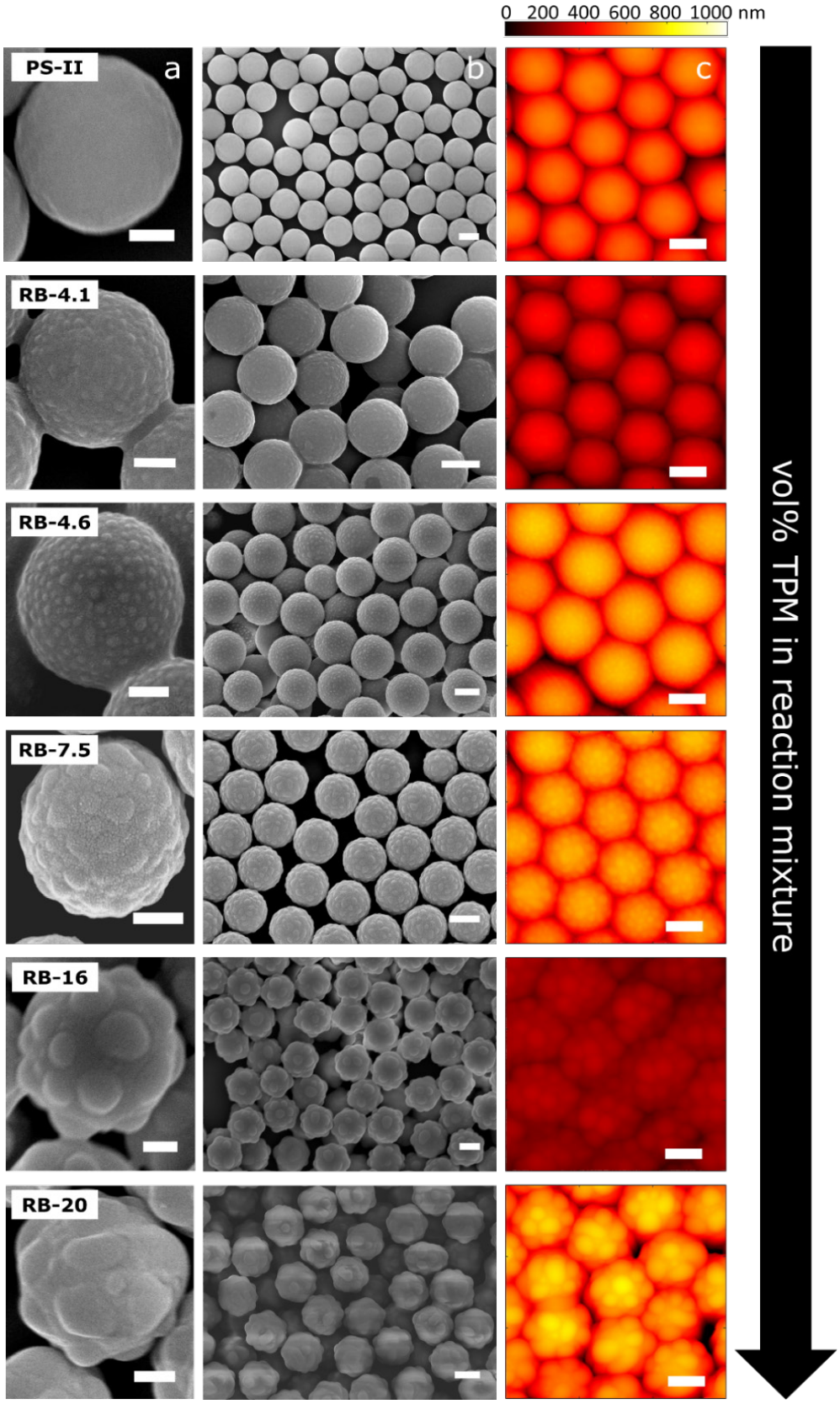

Figure 10. Topographical particle surface characterization by SEM (a,b) and AFM (c). Scalebars: 200 nm (a) and 500 nm (b,c).

The particle-by-particle root-mean-square (RMS) roughness could be extracted from the AFM height maps. The RMS roughness is a suitable parameter to compare the particle roughness since the colloids have similar sizes and the surface morphologies are analogous. For spherical asperities, the height of the asperities determines to the largest extent the RMS, while the asperity density hardly influences RMS.[66] RMS roughnesses of 4.1–20 nm could be achieved by varying the concentration of TPM monomer in the reaction mixture from 0.17 to 0.32 vol%.

The RMS roughness solely describes the surface topography. Thus, a complementary characterization of the patchy rough particles focusing on their chemical composition was carried out. In this regard, thermogravimetric analysis (TGA) was used. In Figure 11a, it can be observed that PS almost completely degrades upon heating the sample to 650°C for 30 min, while 30% of the TPM mass remains. This allowed to calculate the PS/TPM weight ratio in the patchy rough particles.

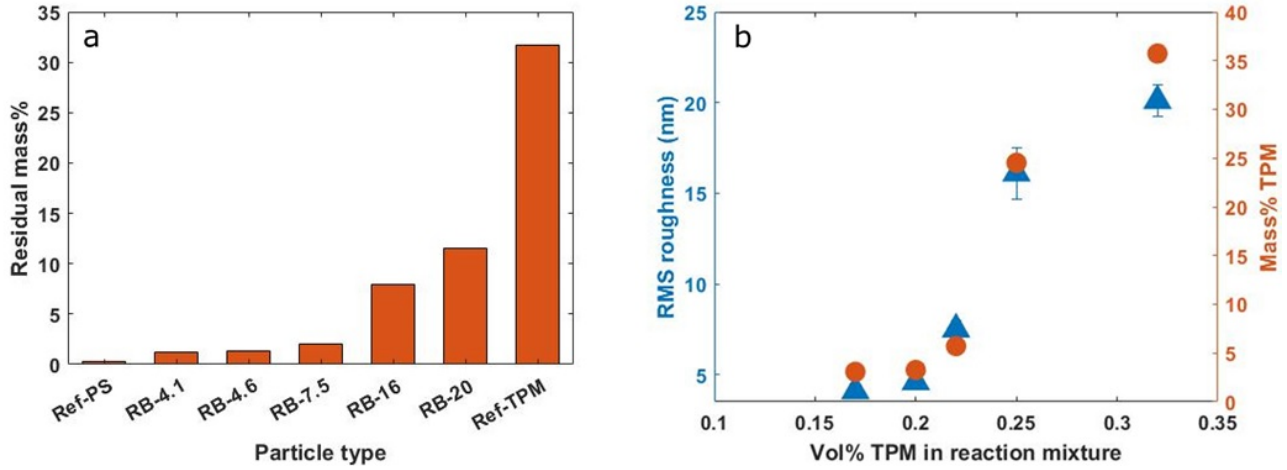

Figure 11. ***Particle characterization by composition and roughness. (a)*** *Residual particle masses after degradation upon calcination. There is no standard deviation reported since the thermogravimetric analysis was only carried out once for each particle.* ***(b)*** *Particle characterization by their RMS roughness as determined with AFM and mass% TPM calculated with thermogravimetric analysis as a function of vol% TPM in the reaction mixture.*

Figure 11b presents the roughness and composition of the particles as function of the TPM volume percentage in the reaction mixture. Both the RMS roughness and mass% TPM exhibit a sigmoidal dependence on the vol% TPM in the reaction mixture. This denotes a strong dependence of particle roughness and composition in a small TPM concentration range. For concentrations lower or higher than this range, the TPM concentration has a milder impact on the particle roughness.

4.3 SURFACE PATCHINESS AND CONTACT ANGLES

To further characterize the chemical heterogeneous nature of the particles, their surface patchiness was estimated using SEM images. 2D and 3D surface patchiness are defined as depicted in Figure 12a. The 2D and the 3D estimation approximate the asperities as their projected area and as spherical caps, respectively. The results of the estimates are presented in Figure 12b. The values for 3D surface patchiness exceed those of the 2D patchiness because the area of the spherical caps is larger than their projected area. Since in practice the asperities have a curvature, the 3D estimation matches the real situation the closest. The 2D estimation captures the chemical partition of the particle surface irrespective of the roughness.

Similar to Figure 11b, the trend of surface patchiness with vol% TPM has a sigmoidal shape. Effectively, the roughness, the composition and the surface patchiness all depend in the same manner on the vol% TPM initially added in the reaction mixture.

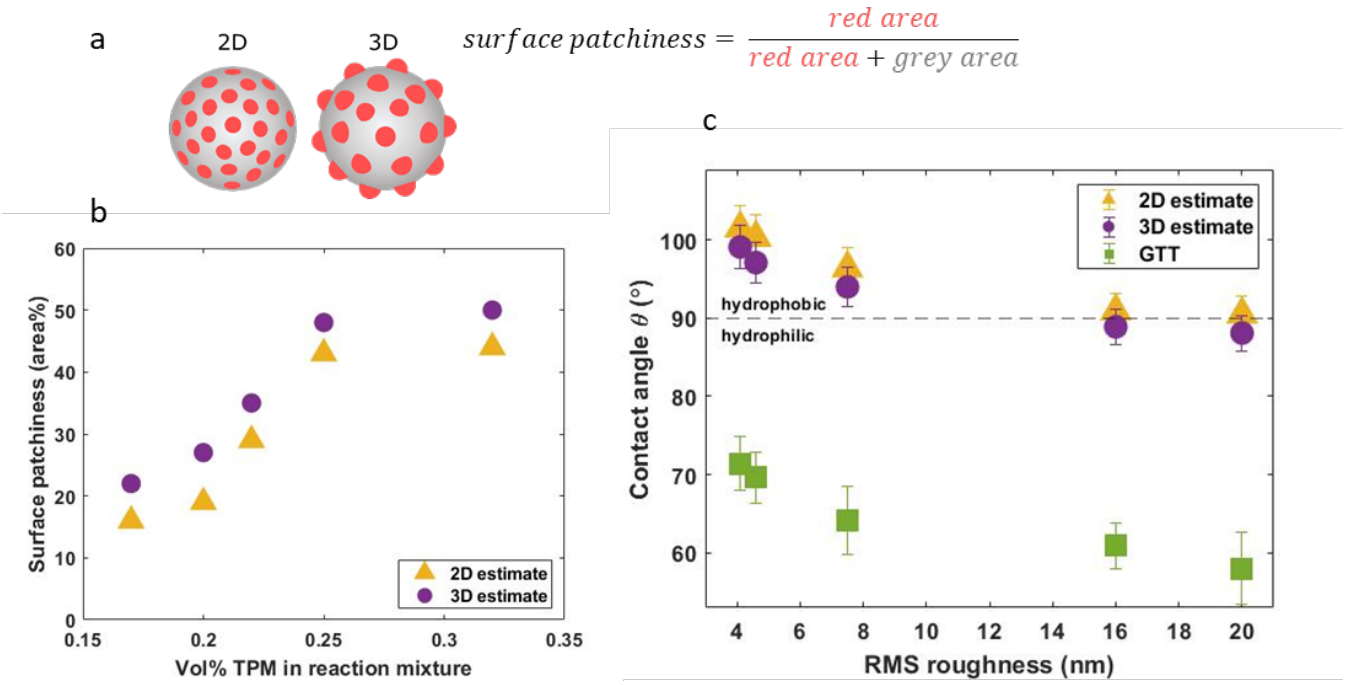

Figure 12. ***Particle characterization by surface patchiness and contact angles. (a)*** *Schematic representation of the definition of 2D and 3D surface patchiness.* ***(b)*** *2D and 3D estimates for the surface patchiness of particles of different compositions.* ***(c)*** *Estimated (from surface patchiness) and measured (by GTT) contact angles of patchy rough particles.*

From the surface patchiness estimations, it is possible to calculate the theoretical contact angles (θ_{theory}) for the rough patchy particles. For this, the contact angles of bear TPM and PS spheres were measured by GTT. The contact angle of the sulfate PS spheres was determined to be 108±7°, which is in good agreement with θs between 101° and 116° reported in literature.[67,73] This means that PS particles are hydrophobic in nature and therefore greatly protruding in the oil phase. Conversely, the contact angle of TPM was 68±7°, which means that it is hydrophilic. Using Cassie's law (see section 2.2) for wetting of heterogeneous surfaces, contact angles for the PS/TPM patchy rough particles were estimated (Figure 12c, yellow triangles and purple circles). Additionally, contact angles of the patchy rough colloids were measured by GTT (Figure 12c, green squares). Remarkably, the measured contact angles are much lower than the estimated wettability values. Effectively, the particles are more hydrophilic than expected purely from their chemical composition. This further corroborates previous observations indicating that the contact line pinning on the roughness features arrests the adsorption (as explained in section 2.2).[24] Contact line pinning can also be occasioned by a sufficiently strong wetting contrast on a single particle surface.[74] These peculiar properties may generate peculiar phenomena when the patchy rough particles are used as Pickering stabilizers.

4.4 EMULSIFICATION AND PHASE INVERSION

To investigate the effect of the particle heterogeneity on the emulsification and formulation of Pickering emulsions, emulsification experiments with particles having different degrees of patchiness were carried out. In particular, the influence of the shear rate, o/w ratio and patchiness on the obtained emulsion type was studied (Figure 13a-I). The emulsions were characterized by macroscopic appearance, bright field optical microscopy and confocal fluorescence microscopy (respectively Figure 13a-II, -III and -IV). The presence of the green fluorescent dye BODIPY in n-decane enabled straight identification of the emulsion type (o/w or w/o, Figure 13a-IV). It should be noted that fluorescent dyes can be surface active and affect emulsions.[75] Therefore, the influence of BODIPY on the water-decane interfacial tensions and on the emulsification was evaluated (see Appendix F). Even though from these experiments it was concluded that in the selected range of concentrations BODIPY does not affect the emulsification, the emulsions were prepared with the lowest possible concentration of BODIPY to avoid any unexpected interference with the emulsification.

According to the Bancroft rule, the phase wherein particles can be stably dispersed constitutes the continuous phase of the emulsion. Interestingly, in this work all particles form stable dispersion in aqueous solutions due to their charge stabilization, despite some cases being inherently hydrophobic (PS, RB-4.1, RB-7.5). Therefore, the inverted emulsions are anti-Bancroft type.

In general, it was observed that rougher particles form with higher success rate emulsion droplets with morphologies that can deviate from circularity compared with smooth particles. This is clearly depicted confronting Figure 13a-IIIA obtained with RB-7.5 particles with Figure 13a-IIIB generated with PS. This is ascribed to the capillary forces between rough particles trapped at the interface arising from the undulated contact line around the particles that generate a 2D network and impart deviatoric rheological properties to the interface.[76,77] Moreover, for the roughest particles (RB-20 and also to some extent RB-16), the amount of emulsion layer was limited. This might be explained by limited adsorption due to a transition from Wenzel wetting for the less rough particles to Cassie-Baxter wetting for the roughest particles. It is posed in literature that in the latter regime, rough particles are less efficient Pickering stabilizers (see section 2.2). Additionally, emulsions created with particles having an extreme degree of patchiness had a discontinuous structure characterized by clusters of droplets. This suggests that very heterogeneous particles have a higher probability of particle bridging, possibly connected to the fact that their contact angle approaches ~60°. More details and investigation of the emulsification challenges encountered with the roughest particles are reported in Appendix G. Because of its limited emulsification, RB-20 was excluded from the phase inversion experiments.

For PS, RB-4.1, RB-7.5 and RB-16, the volume fraction of the water phase φ_{water} and shear rate during emulsification were systematically varied (see Figure 13b). The optical characterization that proves the emulsion types for all the produced emulsions is found in Appendix I. When coexisting w/o and o/w emulsions were observed, the ratio between these emulsion types was assessed from image analysis.

Several interesting trends are reported in Figure 13b. In vertical direction, the effect of shear rate on the emulsion type is shown. The reasoning below is focused on $\varphi_{water} = 0.5$, but can be extended to $\varphi_{water} = 0.3$ and $\varphi_{water} = 0.7$. It can be noticed that the probability of emulsion inversion, in our case from o/w to w/o, enhances with increasing shear rates, i.e. increasing energy input during emulsification. This phenomenon was already described for rough but chemically homogeneous silica and PS particles in emulsions with $\varphi_{water} = 0.5$.[58] Such mechanical phase inversion is ascribed to arrested adsorption of particles at the interface due to contact line pinning on asperities. When a rough, slightly hydrophobic particle is initially dispersed in water, it can form o/w emulsions at low energy input, because the energy barrier that has to be overcome to reach its equilibrium position is not matched. Conversely, higher shear rates can provide enough energy for relaxation of the contact line over the particle, and a w/o emulsion is formed. The same line of thinking is observed for RB-4.1 at $\varphi_{water} = 0.5$ (emulsified from the water). The fact that these particles primarily form o/w emulsions correlates with the contact angle of 71°

found by GTT (section 4.3). The preferred emulsion type would however be w/o as dictated by their surface chemistry according to the contact angle estimated from the surface patchiness calculation. As expected, the emulsion inverts to w/o at higher energy input.

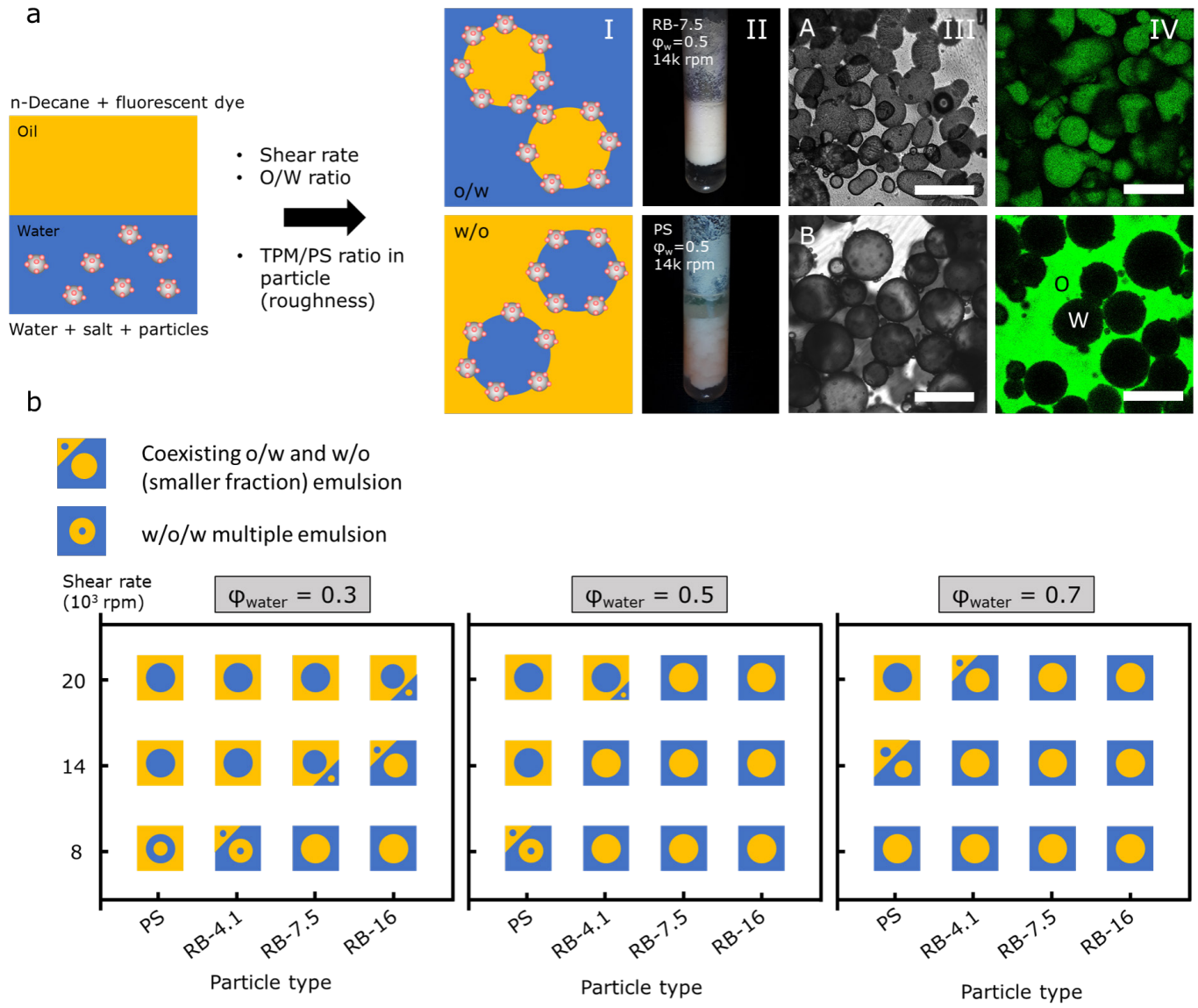

Figure 13. ***Emulsification of patchy rough particles. (a-I)*** *Formulation of emulsions and processing parameters varied to obtain either o/w or w/o emulsion types. a-II to -IV are representative images of o/w (top row) and w/o (bottom row) emulsions.* ***(a-II)*** *Macroscopic photos.* ***(a-III)*** *Bright field microscopy images.* ***(a-IV)*** *Confocal fluorescence microscopy images directly reveal the emulsion type, by addition of BODIPY493/503 in the oil phase. Scalebars: 400μm.* ***(b)*** *Results of emulsion phase inversion experiments for varying shear rate, φ_{water} and particle type.*

Interestingly, RB-7.5 and RB-16 do only form w/o emulsions irrespective of the shear rate for emulsions with φ_{water} = 0.5. For RB-7.5, the contact angle estimated from their surface chemistry is > 90°. In this case it might be that the energy barrier due to contact line pinning on the asperities is too high to be overcome with the emulsification input. Analogous reasoning could apply to RB-16 particles, despite the fact that the estimated contact angle of RB-16 is very close to neutral wettability (88.9°). Therefore, mechanical phase inversion may even be impossible in this. Remarkably, mechanical phase inversion is also observed for PS, despite they are smooth particles and allegedly homogeneous. A kinetic barrier to particle adsorption for PS was already observed.[78] It has been found that the relaxation time for the adsorption was markedly slower than it would be expected from a mere viscous dissipation process. Wang et al.[79] suggested that

this non-ideal behavior can be connected to grafted polymer 'hairs' inducing contact line pinning. The latter can explain the observed mechanical phase inversion of PS-stabilized emulsions.

For the sake of scientific completeness, TPM-stabilized emulsions have been produced and they are shown in Appendix H. TPM forms preferentially o/w emulsions in accordance with its hydrophilicity expressed in the measured contact angle of 68°. Incredibly, for all conditions probed here phase inversion cannot be reached. This suggests that the anchoring of TPM particles at water-oil interfaces is particularly strong.

In reading Figure 13b horizontally per particle type, a second trend is observed that links phase inversion to an increase of φ_{water}. This is known in literature as catastrophic phase inversion.[56] At a shear rate of 20,000 rpm, emulsions with RB-4.1 switch from largely w/o to mainly o/w upon the increase of φ_{water} from 0.5 to 0.7. Emulsions with RB-7.5 and RB-16 undergo such a phase inversion for the increase of φ_{water} = 0.3 to φ_{water} = 0.5, while PS forms w/o emulsions at all volume ratios probed. Dynamic effects in the particle adsorption are supposed to cause the deviation of the inversion point from the thermodynamic critical value of φ_{water} = 0.5 (see section 2.3).[55] Effects of particle roughness might manifest via the difference in particle adsorption dynamics between rough particles and smooth particles. Interestingly, multiple emulsions are observed close to the inversion points as already pointed out in literature.[52,53] The catastrophic phase inversion of emulsions expressed as function of the particle type is even clearer visible in Appendix H.

Most notably, the particle type shifts both the mechanical and catastrophic phase inversion. The onset of mechanically induced phase inversion is highly dependent on the height of the kinetic barrier to equilibrium adsorption. As a consequence, the variation in surface heterogeneity-induced pinning sites among the colloids results in different input energies required to phase invert the emulsions. o/w emulsions become more favored for higher degree of patchiness (decreasing PS/TPM ratio in the particles). Since PS is hydrophobic and TPM is hydrophilic, this behavior is expected. Binks et al. previously found that the volume fraction of water at which catastrophic phase inversion occurs, depends on the particle wettability[80] for particles with a chemically homogeneous surface.[13] Moreover, phase inversion (transitional) from o/w to w/o of emulsions with φ_{water} =0.5 can be induced by addition of hydrophobic silica particles to an emulsion with initially only hydrophilic silica particles and vice versa.[81] Therefrom can be inferred that the emulsion type is determined by the average wettability of all particles present. Accordingly, in the case of composite particles having mixed wettability on the same surface, it is reasonable to conclude that the average wettability of the single particles determines the preferred emulsion type.

Thus, we can conclude that the onsets of mechanical and catastrophic phase inversion depend on the level of heterogeneity of the particle surface. Systematic variations of the shear rate, o/w ratio and particle type in emulsification experiments reveal the effect of particle heterogeneity on the processing and formulation of emulsions.

5 CONCLUSIONS

Heterogeneous patchy rough colloids composed of PS cores decorated with organosilicate asperities can be fabricated with tunable surface roughness and composition. The proposed wet chemical process is reliable and ensures the production of large amounts of monodisperse rough colloidal composites with controlled patchiness degree. The latter is achieved by tuning the sole amount of reactive organosilicate (TPM) in the reaction mixture at selected pH and nuclei concentration. In this fashion, patchy rough particles with root-mean-square surface roughness ranging between 4.1 and 20 nm and compositions of 3.1 to 36 mass% of TPM were obtained. The roughness of the particles was characterized scanning individual colloidal particles with AFM. An estimate of their composition expressed in mass% of TPM could be obtained from thermogravimetric analysis. SEM image analysis allowed for an estimation of the surface patchiness of the particles. The comparison of contact angles estimated from surface patchiness with contact angles measured by GTT indicates that the adsorption of patchy rough colloids at liquid interfaces can be arrested by contact line pinning at heterogeneity sites. In this system, surface roughness and the chemical nature of the surface are coupled. Interestingly, the fabricated patchy rough particles can be used as Pickering emulsifiers of water/n-decane systems. Systematic variations in the emulsification shear rate, o/w ratio and particle type corroborate the influence of the particle heterogeneity on the processing and formulation of emulsions. It has been confirmed that mechanically induced phase inversion of the emulsions can be achieved by colloidal particles presenting a kinetically arrested adsorption pathway. Additionally, light has been shed on the role that kinetic effects at a single particle level have on the phase inversion of Pickering emulsions. The output of the work expands the previous state-of-the-art research and opens a future and fruitful scenario for the use of non-ideal colloidal systems for smart formulations, on-demand switchable emulsions and uncharted recovery strategies.

6 OUTLOOK

The fabrication of the PS/TPM patchy rough particles can be even more appealing by considering the flexible surface chemistry of TPM. TPM silanol surface groups can namely easily be functionalized by chemisorption of many different silicates.[82] This creates the opportunity to specifically modify surface patches giving access to a more versatile particle surface chemistry.

With respect to emulsification, it was observed that selected formulations of patchy rough particles form emulsions with coexisting emulsion types (both o/w and w/o). It would be worthwhile to study the emulsion evolution over time. This is one important step to draw conclusions regarding the long-term stability of the Pickering emulsions stabilized by patchy rough colloids.

A natural extension of the study on the catastrophic phase inversion of emulsions with patchy rough particles is going towards higher and lower φ_{water} to cover the whole volume ratio range.

In addition, the research on phase inversion would be more exhaustive when also emulsification with particles initially dispersed in the oil would be considered. It is anticipated that because of arrested adsorption, the phase inversion diagram would be rigorously different, and more knowledge could be gathered about the chemical preferred wettability of the particles. However, lack of charge stabilization and swelling of PS in the oil phase might hinder the formation of stable dispersions of the particles in oil.

As a reference, it could be useful to examine the emulsification behavior of particles with smooth surfaces with a range of contact angles in between PS and TPM. Such particles would then possibly resemble the chemical nature of the patchy rough particles, without displaying the roughness effects.

The other way around, it would be interesting to investigate the effect of purely roughness on catastrophic phase inversion. The locus of catastrophic phase inversion is related to several kinetic factors regarding particle adsorption.[55] Since particle adsorption dynamics is probably different for rough particles than for smooth particles,[77] it might be interesting to identify possible differences. It should for example be possible to synthesize all-TPM rough particles,[61] which could be suitable to study the catastrophic phase inversion as a function of the sole surface roughness.

To study the adsorption kinetics of the patchy rough particles on droplets more in depth, binodal decomposition of a mixture in the presence of the particles could be observed and analyzed with real-time microscopy. Evolution of the droplet size during this process could be monitored, thereby providing an estimate of the efficiency of the particles as Pickering stabilizers.

Generally, the investigation of particles at interfaces covers three aspects: motion, interactions, and adsorption. The latter aspect is connected with wetting, and is studied predominantly in this work. The study of particle dynamics on a droplet could be enabled by the possibility to make the particles fluorescent during their fabrication. Interactions of particles at the interface become apparent for example in altered viscosity of the interface.[47] Interfacial rheology studies on interfaces laden with the patchy rough particles might shed a light on this.

In connection with the interfacial rheology of particle-laden interfaces, it might be interesting to investigate the role of particle concentration on the stability of emulsions. It was found that the yield stress of an interface is more directive for emulsion stability than the surface coverage.[49] Moreover, particle dynamics supposedly plays a role in the stabilization of weakly-covered emulsion droplets.[77,83] Study might focus on how this works for heterogeneous particles of for example the type used in this work.

In the end, more fundamental insights and knowledge about heterogeneous particles as Pickering stabilizers such as the rough patchy particles from this work may be of use in chemical, biomedical and industrial applications.

ACKNOWLEDGEMENTS

MZ acknowledges the Swiss National Science Foundation (SNSF) for the financial support through the Early post.Doc mobility grant P2EZP2-178502.

F. Dekker and L. C. Post are acknowledged for their help with respectively SEM and AFM.

I am very grateful to my supervisor Dr. Michele Zanini for his guidance and support throughout my entire research project.

I would like to thank Prof. Willem Kegel and the weekly brainstorm group for suggestions during the course of my research.

Finally, I must express my gratitude to FCC for creating the environment in which I could carry out this Masters research project.

LAY SUMMARY (NEDERLANDS)

Een emulsie is een mengsel van twee eigenlijk niet mengbare vloeistoffen, meestal olie en water. Wanneer je olie en water bij elkaar doet, zullen zich normaalgesproken twee fasen vormen: een waterlaag met daarop een olielaag. Als je hard schudt, mengen de olie en water fasen even doordat de ene fase druppeltjes vormt in de andere, maar al snel ontstaan er weer gescheiden lagen. In een emulsie is iets toegevoegd wat ervoor zorgt dat de druppeltjes van de ene fase niet meer kunnen samensmelten en scheiden tot een continue fase. Mayonaise is bijvoorbeeld een olie-in-water emulsie waar eiwitten de zogenaamde emulgatoren zijn die oliedruppeltjes stabiliseren in water. Ook veel andere producten die je tegenkomt in het dagelijks leven worden gemaakt op basis van emulsies, zoals verschillende voedingsproducten en cosmetica.

Bij het maken van emulsies is er een groot aanbod aan mogelijke emulgatoren. Heel gebruikelijk zijn surfactanten: kleine stoffen die op het grensvlak tussen twee vloeistoffen gaan zitten. Deze surfactant moleculen zijn grofweg 100.000x kleiner dan de dikte van een mensenhaar. Ook vaste deeltjes kunnen op vloeistofgrensvlakken gaan zitten. Zulke deeltjes zijn zo'n 100-1000x kleiner dan de dikte van een mensenhaar en worden in het algemeen aangeduid als colloïden. Rigide lagen van colloïden op bijvoorbeeld oliedruppels in water zorgen ervoor dat de oliedruppels gescheiden blijven, en stabiliseren zo de emulsie. Zo'n emulsie gestabiliseerd door vaste deeltjes heet een Pickering emulsie, genoemd naar een pionier op het gebied van dit soort emulsies.

Er wordt vaak onderzoek gedaan naar de aard en eigenschappen van Pickering emulsies met deeltjes die beschouwd worden als gladde bollen die uit één materiaal bestaan. Maar in realistische of natuurlijke systemen zijn de deeltjes niet noodzakelijk zo. Ook kunnen deeltjes met een andere vorm en samenstelling interessante eigenschappen geven aan de emulsies die ze produceren.

Om meer inzicht te krijgen in de emulsificatie met zulke heterogene deeltjes, worden in dit werk ruwe colloïden bestaande uit twee materialen gefabriceerd als emulgatoren: zogenaamde 'framboos-achtige deeltjes'. Door deeltjes van verschillende ruwheid en samenstelling te gebruiken, wordt de invloed van deze eigenschappen op de vorming van emulsies duidelijk. Afhankelijk van de heterogeniteit van de deeltjes, worden olie-in-water of water-in-olie emulsies gevormd bij verschillende manieren van emulsies produceren. Dit onderzoek draagt bij aan een breder begrip van de invloed van heterogeniteit van deeltjes op emulsificatie.

BIBLIOGRAPHY

1. Dickinson, E. Food emulsions and foams: Stabilization by particles. *Curr. Opin. Colloid Interface Sci.* **15**, 40–49 (2010).
2. Sharma, S. & Sarangdevot, K. Nanoemulsions For Cosmetics. *IJARPB* **2**, 408–415 (2012).
3. Mizutani, T., Arai, K., Miyamoto, M. & Kimura, Y. Application of silica-containing nano-composite emulsion to wall paint: A new environmentally safe paint of high performance. *Prog. Org. Coatings* **55**, 276–283 (2006).
4. Li, Z., Xiao, M., Wang, J. & Ngai, T. Pure protein scaffolds from pickering high internal phase emulsion template. *Macromol. Rapid Commun.* **34**, 169–174 (2013).
5. Yang, Y. *et al.* An overview of pickering emulsions: Solid-particle materials, classification, morphology, and applications. *Front. Pharmacol.* **8**, 287 (2017).
6. Perazzo, A., Preziosi, V. & Guido, S. Phase inversion emulsification: Current understanding and applications. *Adv. Colloid Interface Sci.* **222**, 581–599 (2015).
7. Linke, C. & Drusch, S. Pickering emulsions in foods-opportunities and limitations. *Crit. Rev. Food Sci. Nutr.* **58**, 1971–1985 (2018).
8. Binks, B. P. Particles as surfactants - similarities and differences. *Curr. Opin. Colloid Interface Sci.* **7**, 21–41 (2002).
9. Ramsden, W. Separation of solids in the surface-layers of solutions and 'suspensions' (observations on surface-membranes, bubbles, emulsions, and mechanical coagulation).—Preliminary account. *Proc. R. Soc. London* **72**, 156–164 (1904).
10. Pickering, S. U. CXCVI. - Emulsions. *J. Chem. Soc., Trans.* **91**, 2001–2021 (1907).
11. Calabrese, V., Courtenay, J. C., Edler, K. J. & Scott, J. L. Pickering emulsions stabilized by naturally derived or biodegradable particles. *Curr. Opin. Green Sustain. Chem.* **12**, 83–90 (2018).
12. Binks, B. P. & Rodrigues, J. A. Inversion of emulsions stabilized solely by ionizable nanoparticles. *Angew. Chemie - Int. Ed.* **44**, 441–444 (2005).
13. Binks, B. P. & Fletcher, P. D. I. Particles Adsorbed at the Oil-Water Interface: A Theoretical Comparison between Spheres of Uniform Wettability and 'Janus' Particles. *Langmuir* **17**, 4708–4710 (2001).
14. Jeon, T. Y. & Hong, J. S. Stabilization of O/W emulsion with hydrophilic/hydrophobic clay particles. *Colloid Polym. Sci.* **292**, 2939–2947 (2014).
15. Guillot, S., Bergaya, F., de Azevedo, C., Warmont, F. & Tranchant, J. F. Internally structured pickering emulsions stabilized by clay mineral particles. *J. Colloid Interface Sci.* **333**, 563–569 (2009).
16. Du, J. & O'reilly, R. K. Anisotropic particles with patchy, multicompartment and Janus architectures: preparation and application. *Chem. Soc. Rev* **40**, 2402–2416 (2011).
17. Yusoff, A. & Murray, B. S. Modified starch granules as particle-stabilizers of oil-in-water emulsions. *Food Hydrocoll.* **25**, 42–55 (2011).
18. McClements, D. J. & Jafari, S. M. Improving emulsion formation, stability and performance using mixed emulsifiers: A review. *Adv. Colloid Interface Sci.* **251**, 55–79 (2018).
19. Jiang, S. *et al.* Janus Particle Synthesis and Assembly. *Adv. Mater.* **22**, 1060–1071 (2010).
20. Ji, X. *et al.* Ionic liquid functionalized Janus nanosheets. *Chem. Commun.* **50**, 5706–5709 (2014).
21. Mejia, A. F. *et al.* Pickering emulsions stabilized by amphiphilic nano-sheets. *Soft Matter* **8**, 10245 (2012).
22. Madivala, B., Vandebril, S., Fransaer, J. & Vermant, J. Exploiting particle shape in solid stabilized emulsions. *Soft Matter* **5**, 1717–1727 (2009).
23. Wu, D., Chew, J. W. & Honciuc, A. Polarity reversal in homologous series of surfactant-

free janus nanoparticles: Toward the next generation of amphiphiles. *Langmuir* **32**, 6376–6386 (2016).

24. Zanini, M. *et al.* Universal emulsion stabilization from the arrested adsorption of rough particles at liquid-liquid interfaces. *Nat. Commun.* **8**, 1–9 (2017).
25. Bradley, L. C., Chen, W., Stebe, K. J. & Lee, D. Janus and patchy colloids at fluid interfaces. *Curr. Opin. Colloid Interface Sci.* **30**, 25–33 (2017).
26. Bouchama, F., van Aken, G. A., Autin, A. J. E. & Koper, G. J. M. On the mechanism of catastrophic phase inversion in emulsions. *Colloids Surfaces A Physicochem. Eng. Asp.* **231**, 11–17 (2003).
27. Mira, I. *et al.* Emulsion Catastrophic Inversion from Abnormal to Normal Morphology. 2. Effect of the Stirring Intensity on the Dynamic Inversion Frontier. *Ind. Eng. Chem. Res.* **42**, 57–61 (2003).
28. Spiecker, P. M., Gawrys, K. L., Trail, C. B. & Kilpatrick, P. K. Effects of petroleum resins on asphaltene aggregation and water-in-oil emulsion formation. *Colloids Surfaces A Physicochem. Eng. Asp.* **220**, 9–27 (2003).
29. Hunter, T. N., Pugh, R. J., Franks, G. V. & Jameson, G. J. The role of particles in stabilising foams and emulsions. *Adv. Colloid Interface Sci.* **137**, 57–81 (2008).
30. Widerström, E. & Öhman, R. Mayonnaise Quality and Catastrophic Phase Inversion. (Lund University, 2017).
31. Whitby, C. & Wanless, E. Controlling Pickering Emulsion Destabilisation: A Route to Fabricating New Materials by Phase Inversion. *Materials (Basel).* **9**, 626 (2016).
32. Bonn, D., Eggers, J., Indekeu, J., Meunier, J. & Rolley, E. Wetting and spreading. *Rev. Mod. Phys.* **81**, 739 (2009).
33. Nosonovsky, M. & Ramachandran, R. Geometric interpretation of surface tension equilibrium in superhydrophobic systems. *Entropy* **17**, 4684–4700 (2015).
34. Chevalier, Y. & Bolzinger, M. A. Emulsions stabilized with solid nanoparticles: Pickering emulsions. *Colloids Surfaces A Physicochem. Eng. Asp.* **439**, 23–34 (2013).
35. Aveyard, R., Binks, B. P. & Clint, J. H. Emulsions stabilised solely by colloidal particles. *Adv. Colloid Interface Sci.* **100**–**102**, 503–546 (2003).
36. Jennings, H. Y. The effect of temperature and pressure on the interfacial tension of benzene-water and normal decane-water. *J. Colloid Interface Sci.* **24**, 323–329 (1967).
37. Arditty, S., Whitby, C. P., Binks, B. P., Schmitt, V. & Leal-Calderon, F. Some general features of limited coalescence in solid-stabilized emulsions. *Eur. Phys. J. E* **11**, 273–281 (2003).
38. Alison, L. *et al.* Pickering and Network Stabilization of Biocompatible Emulsions Using Chitosan-Modified Silica Nanoparticles. *Langmuir* **32**, 13446–13457 (2016).
39. Cassie, A. B. D. Contact angles. *Discuss. Faraday Soc.* **3**, 11–16 (1948).
40. San-Miguel, A. & Behrens, S. H. Influence of nanoscale particle roughness on the stability of pickering emulsions. *Langmuir* **28**, 12038–12043 (2012).
41. Mable, C. J., Warren, N. J., Thompson, K. L., Mykhaylyk, O. O. & Armes, S. P. Framboidal ABC triblock copolymer vesicles: a new class of efficient Pickering emulsifier. *Chem. Sci.* **6**, 6179–6188 (2015).
42. Stamou, D., Duschl, C. & Johannsmann, D. Long-range attraction between colloidal spheres at the air-water interface: The consequence of an irregular meniscus. *Phys. Rev. E - Stat. Physics, Plasmas, Fluids, Relat. Interdiscip. Top.* **62**, 5263–5272 (2000).
43. Loudet, J. C. & Pouligny, B. How do mosquito eggs self-assemble on the water surface? *Eur. Phys. J. E* **34**, (2011).
44. Department of Physics and Astronomy. So what is a hexacontatretapole moment, anyway? *University of Nebraska* (2014). Available at: http://physics.unl.edu/~tgay/content/multipoles.html. (Accessed: 4th December 2019)
45. Kralchevsky, P. A. & Denkov, N. D. Capillary forces and structuring in layers of collid particles. *Curr. Opin. Colloid Interface Sci.* **6**, 383–401 (2001).

46. Soligno, G., Dijkstra, M. & van Roij, R. The equilibrium shape of fluid-fluid interfaces: Derivation and a new numerical method for Young's and Young-Laplace equations. *J. Chem. Phys.* **141**, 244702 (2014).
47. Botto, L., Lewandowski, E. P., Cavallaro, M. & Stebe, K. J. Capillary interactions between anisotropic particles. *Soft Matter* **8**, 9957–9971 (2012).
48. van Hooghten, R., Imperiali, L., Boeckx, V., Sharma, R. & Vermant, J. Rough nanoparticles at the oil-water interfaces: Their structure, rheology and applications. *Soft Matter* **9**, 10791–10798 (2013).
49. Beltramo, P. J. *et al.* Arresting dissolution by interfacial rheology design. *PNAS* **114**, 10373–10378 (2017).
50. Binks, B. P., Murakami, R., Armes, S. P. & Fujii, S. Temperature-induced inversion of nanoparticle-stabilized emulsions. *Angew. Chemie - Int. Ed.* **44**, 4795–4798 (2005).
51. Golemanov, K., Tcholakova, S., Kralchevsky, P. A., Ananthapadmanabhan, K. P. & Lips, A. Latex-Particle-Stabilized Emulsions of Anti-Bancroft Type. *Langmuir* **22**, 4968–4977 (2006).
52. Clegg, P. S., Tavacoli, J. W. & Wilde, P. J. One-step production of multiple emulsions: microfluidic, polymer-stabilized and particle-stabilized approaches. *Soft Matter* **12**, 998 (2016).
53. Binks, B. P. & Rodrigues, J. A. Types of Phase Inversion of Silica Particle Stabilized Emulsions Containing Triglyceride Oil. *Langmuir* **19**, 4905–4912 (2003).
54. Tadros, T. F. Emulsion Formation, Stability, and Rheology. in *Emulsion Formation and Stablility* (ed. Tadros, T. F.) (WILEY-VCH Verlag GmbH & Co. KGaA, 2013).
55. Kralchevsky, P. A., Ivanov, I. B., Ananthapadmanabhan, K. P. & Lips, A. On the Thermodynamics of Particle-Stabilized Emulsions: Curvature Effects and Catastrophic Phase Inversion. *Langmuir* **21**, 50–63 (2005).
56. Binks, B. P. & Lumsdon, S. O. Catastrophic Phase Inversion of Water-in-Oil Emulsions Stabilized by Hydrophobic Silica. *Langmuir* **16**, 2539–2547 (2000).
57. Nonomura, Y. & Kobayashi, N. Phase inversion of the Pickering emulsions stabilized by plate-shaped clay particles. *J. Colloid Interface Sci.* **330**, 463–466 (2009).
58. Zanini, M. *et al.* Mechanical phase inversion of Pickering emulsions via metastable wetting of rough colloids. *Soft Matter* **15**, 7888 (2019).
59. Zhang, F., Cao, L. & Yang, W. Preparation of Monodisperse and Anion-Charged Polystyrene Microspheres Stabilized with Polymerizable Sodium Styrene Sulfonate by Dispersion Polymerization. *Macromol. Chem. Phys.* **211**, 744–751 (2010).
60. Kawaguchi, S. & Ito, K. Dispersion Polymerization. *Adv. Polym. Sci* **175**, 299–328 (2005).
61. Liu, Y. *et al.* Core–Shell Particles for Simultaneous 3D Imaging and Optical Tweezing in Dense Colloidal Materials. *Adv. Mater.* **28**, 8001–8006 (2016).
62. van der Wel, C. *et al.* Preparation of Colloidal Organosilica Spheres through Spontaneous Emulsification. *Langmuir* **33**, 8174–8180 (2017).
63. Reusch, W. Free Radical Polymerization. *Chemistry LibreTexts* (2015). Available at: https://chem.libretexts.org/LibreTexts/Purdue/Purdue_Chem_26100%3A_Organic_Chemistry_I_(Wenthold)/Chapter_08%3A_Reactions_of_Alkenes/8.7.%09Polymerization/Free_Radical_Polymerization. (Accessed: 26th September 2018)
64. Denkov, N. D. *et al.* Mechanism of Formation of Two-Dimensional Crystals from Latex Particles on Substrates. *Langmuir* **8**, 3183–3190 (1992).
65. Bhushan, B. Surface roughness analysis and measurement techniques. in *Modern Tribology Handbook: Volume One: Principles of Tribology* 49–119 (CRC Press LLC, 2001). doi:10.1201/9780849377877.ch2
66. Zanini, M., Hsu, C. P., Magrini, T., Marini, E. & Isa, L. Fabrication of rough colloids by heteroaggregation. *Colloids Surfaces A Physicochem. Eng. Asp.* **532**, 116–124 (2017).
67. Paunov, V. N. Novel Method for Determining the Three-Phase Contact Angle of Colloid Particles Adsorbed at Air-Water and Oil-Water Interfaces. *Langmuir* **19**, 7970–7976

(2003).

68. Nikolov, A. D. *et al.* Superspreading driven by Marangoni flow. *Adv. Colloid Interface Sci.* **96**, 325–338 (2002).
69. Cayre, O. J. & Paunov, V. N. Contact Angles of Colloid Silica and Gold Particles at Air-Water and Oil-Water Interfaces Determined with the Gel Trapping Technique. *Langmuir* **20**, 9594–9599 (2004).
70. Binks, B. P., Duncumb, B. & Murakami, R. Effect of pH and Salt Concentration on the Phase Inversion of Particle-Stabilized Foams. *Langmuir* **23**, 9143–9146 (2007).
71. Tadros, T. F. General Principles of Colloid Stability and the Role of Surface Forces. in *Colloid Stability* (Wiley-VCH Verlag GmbH & Co. KGaA, 2007).
72. Zhang, X. *et al.* Controllable synthesis of raspberry-like PS-SiO_2 nanocomposite particles via Pickering emulsion polymerization †. *RSC Adv.* **8**, 3910–3918 (2018).
73. Maestro, A., Guzmán, E., Ortega, F. & Rubio, R. G. Contact angle of micro- and nanoparticles at fluid interfaces. *Curr. Opin. Colloid Interface Sci.* **19**, 355–367 (2014).
74. De Gennes, P. G. Wetting: Statics and dynamics. *Rev. Mod. Phys.* **57**, 827–863 (1985).
75. Thijssen, J. H. J., Schofield, A. B. & Clegg, P. S. How do (fluorescent) surfactants affect particle-stabilized emulsions? *Soft Matter* **7**, 7965 (2011).
76. Danov, K. D. & Kralchevsky, P. A. Capillary forces between particles at a liquid interface: General theoretical approach and interactions between capillary multipoles. *Adv. Colloid Interface Sci.* **154**, 91–103 (2010).
77. Vignati, E. & Piazza, R. Pickering Emulsions: Interfacial Tension, Colloid Layer Morphology, and Trapped-Particle Motion. *Langmuir* **19**, 6650–6656 (2003).
78. Kaz, D. M., McGorty, R., Mani, M., Brenner, M. P. & Manoharan, V. N. Physical ageing of the contact line on colloidal particles at liquid interfaces. *Nat. Mater.* **11**, 138–142 (2012).
79. Wang, A., McGorty, R., Kaz, D. M. & Manoharan, V. N. Contact-line pinning controls how quickly colloidal particles equilibrate with liquid interfaces. *Soft Matter* **12**, 8958–8967 (2016).
80. Binks, B. P. & Lumsdon, S. O. Influence of Particle Wettability on the Type and Stability of Surfactant-Free Emulsions. *Langmuir* **16**, 8622–8631 (2000).
81. Binks, B. P. & Lumsdon, S. O. Transitional phase inversion of solid-stabilized emulsions using particle mixtures. *Langmuir* **16**, 3748–3756 (2000).
82. Arkles, B. Hydrophobicity, Hydrophilicity and Silane Surface Modification. *Gelest, Inc.* (2006).
83. Gautier, F. *et al.* Pickering emulsions with stimulable particles: from highly- to weakly covered interfaces. *Phys. Chem. Chem. Phys* **9**, 6455–6462 (2007).
84. Berry, J. D., Neeson, M. J., Dagastine, R. R., Chan, D. Y. C. & Tabor, R. F. Measurement of surface and interfacial tension using pendant drop tensiometry. *J. Colloid Interface Sci.* **454**, 226–237 (2015).
85. Wang, H., Singh, V. & Behrens, S. H. Image Charge Effects on the Formation of Pickering Emulsions. *J. Phys. Chem. Lett* **3**, 46 (2012).

APPENDICES

APPENDIX A. HOMOGENEOUS NUCLEATION OF TPM

To verify that TPM particle size increases with increasing volume fraction of TPM in the reaction mixture at constant pH, TPM particles were produced via homonucleation in the following manner: 25, 30, 35, 42 or 50 µL TPM was added to 16 mL water in a 50 mL polypropylene centrifuge tube brought at pH 10.4 by addition of NH_3. After agitation on a tumbling table at 150 rpm for 90 min, 8 mg AIBN was added. The tube was brought under N_2 and tumbled in an oil bath (80°C) for 2 hours. After washing the resulting particles by centrifugation, SEM images (Phenom ProX) were taken from which the particle sizes were determined. Figure A 1 shows the observed nearly linear increase of TPM particle size with volume fraction of TPM in the reaction mixture. This principle was exploited for the synthesis of the patchy rough particles.

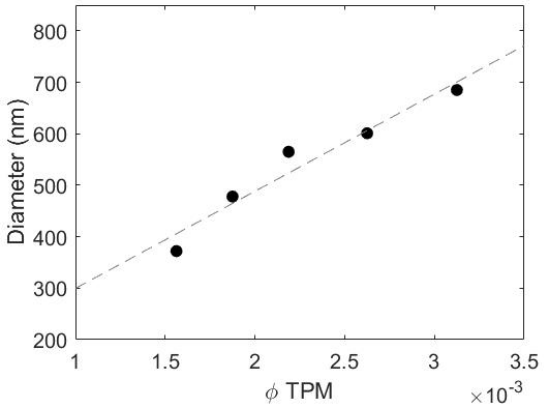

Figure A 1. Homogeneous nucleation of TPM. The graph shows the increase in TPM particle size with increasing volume fraction (Φ) TPM in the reaction mixture.

TPM particles for GTT and emulsification

TPM particles of 797±109 nm in diameter were produced by homogeneous nucleation of TPM in a scaled-up synthesis yielding over half a gram of particles. For this, 2.7 mL TPM was added to 800 mL water and 200 µL NH_3 in a Teflon bottle. After agitation of the mixture for 2 hours on a tumbling table (to accommodate the formation of TPM droplets) the mixture was transferred to a 2L round-bottomed flask. To this, 260 mg of the polymerization initiator AIBN was added and the flask was deoxygenated with N_2. The polymerization of the TPM spheres was carried out under magnetic stirring in an oil bath (80°C) for 2 hours. The resulting particles were washed three times by centrifugation at 3270 × g. The particle size was determined from SEM (Phenom ProX), see Figure A 2. These particles were used for GTT contact angle measurements and for producing reference emulsions.

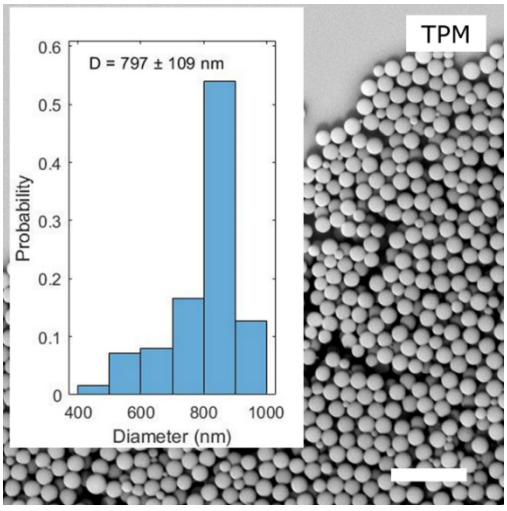

Figure A 2. Size distribution of the TPM particles determined from the SEM image. Scale bar: 4 µm.

APPENDIX B. TGA CALCULATION

For the estimation of the mass% TPM in the patchy rough particles, first the residual masses upon calcination of pure PS and TPM were determined. With these quantities and the dry and residual masses of the patchy rough particles, the composition of these particles in mass% TPM was calculated.

Calculated quantities from reference measurements:

-Pure PS residual mass fraction (PSrMf)

-Pure TPM residual mass fraction (TPMrMf)

Weighed quantities from patchy rough particle measurements:

-Particle mass after drying (drym)

-Residual mass after calcination (resm)

Since the patchy rough particles are composed of both PS and TPM, the drym consists of the dried TPM mass (dTPMm) and dried PS mass (dPSm), and the resm consists of the residual TPM mass (rTPMm) and residual PS mass (rPSm). In equations:

$$dPSm + dTPMm = drym$$

$$rPSm + rTPMm = resm$$

These equations are coupled by:

$$PSrMf * dPSm = rPSm$$

$$TPMrMf * dTPMm = rTPMm$$

Combining these equations gives the following system of equations, solvable for dTPMm:

$$PSrMf * (drym - dTPMm) = resm - rTPMm$$

$$rTPMm = TPMrMf * dTPMm$$

The mass% TPM in the patchy rough particles is then dTPMm/drym*100%.

APPENDIX C. SEM IMAGES FOR SURFACE PATCHINESS

Figure A 3 and Figure A 4Figure A 1 show representative SEM images from which the surface patchiness of the patchy rough particles was estimated. Each left image shows the asperity size measurement and each right image the estimation of the number of asperities on a sphere.

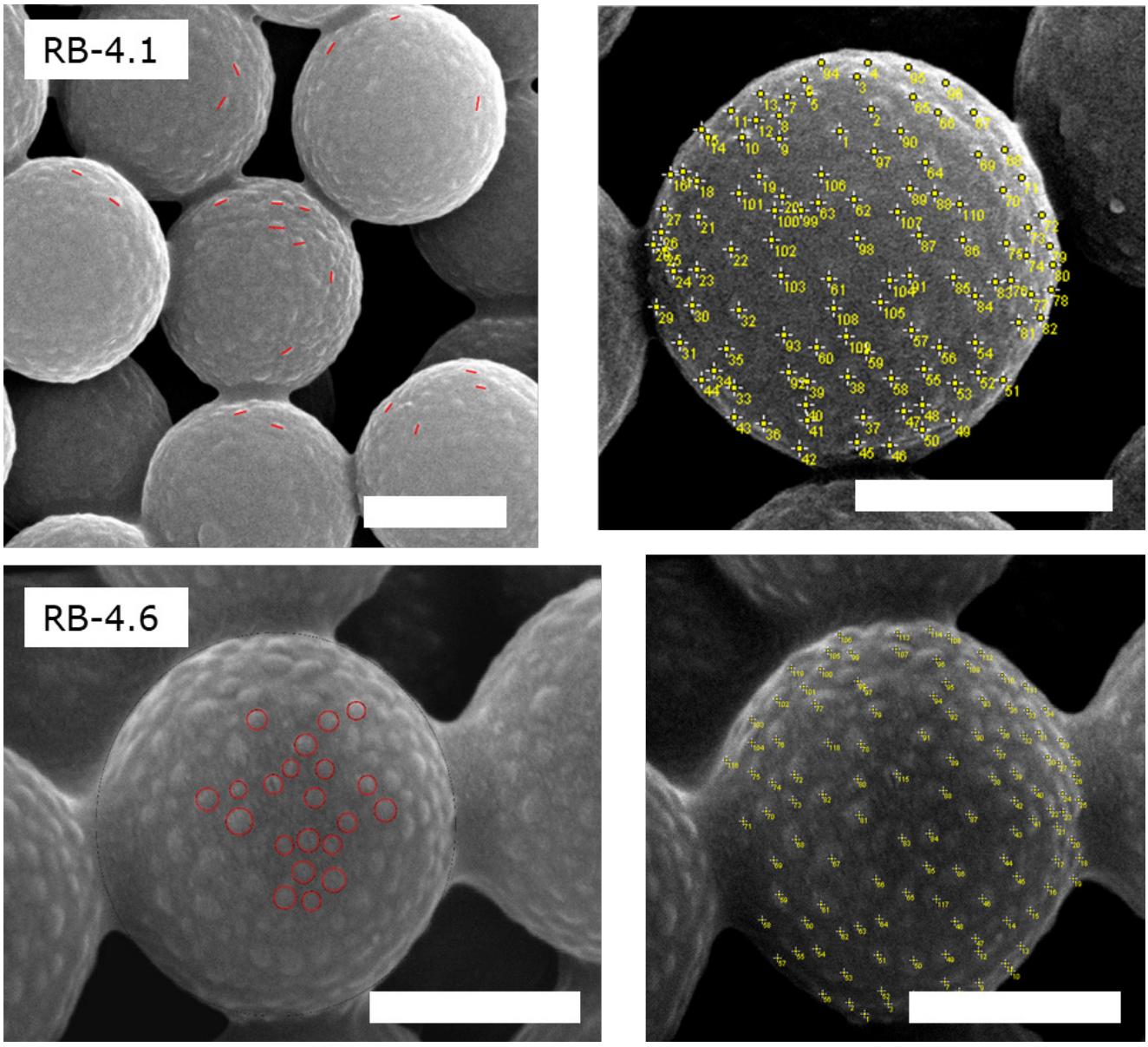

Figure A 3. Representative SEM images for surface patchiness estimation of RB-4.1 and RB-4.6. Scalebars: 500 nm.

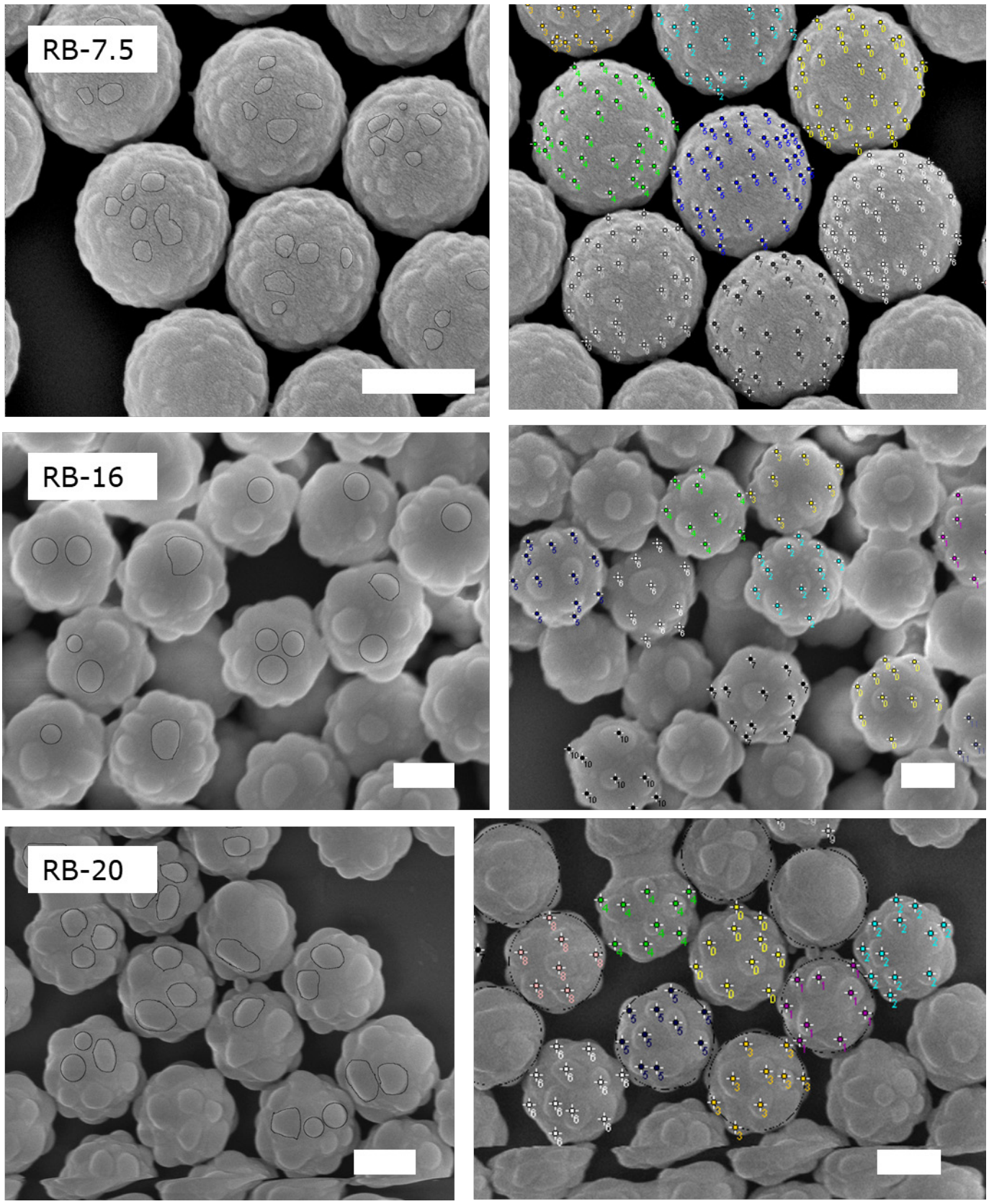

Figure A 4. Representative SEM images for surface patchiness estimation of RB-7.5, RB-16 and RB-20. Scalebars: 500 nm.

APPENDIX D. GTT CONTACT ANGLE CALCULATION

This section contains details on the contact angle calculations from SEM images of interface replicas produced by GTT. Figure A 5 shows representative images used for the contact angle calculations. At least 70 particles of each particle type were involved in the calculations.

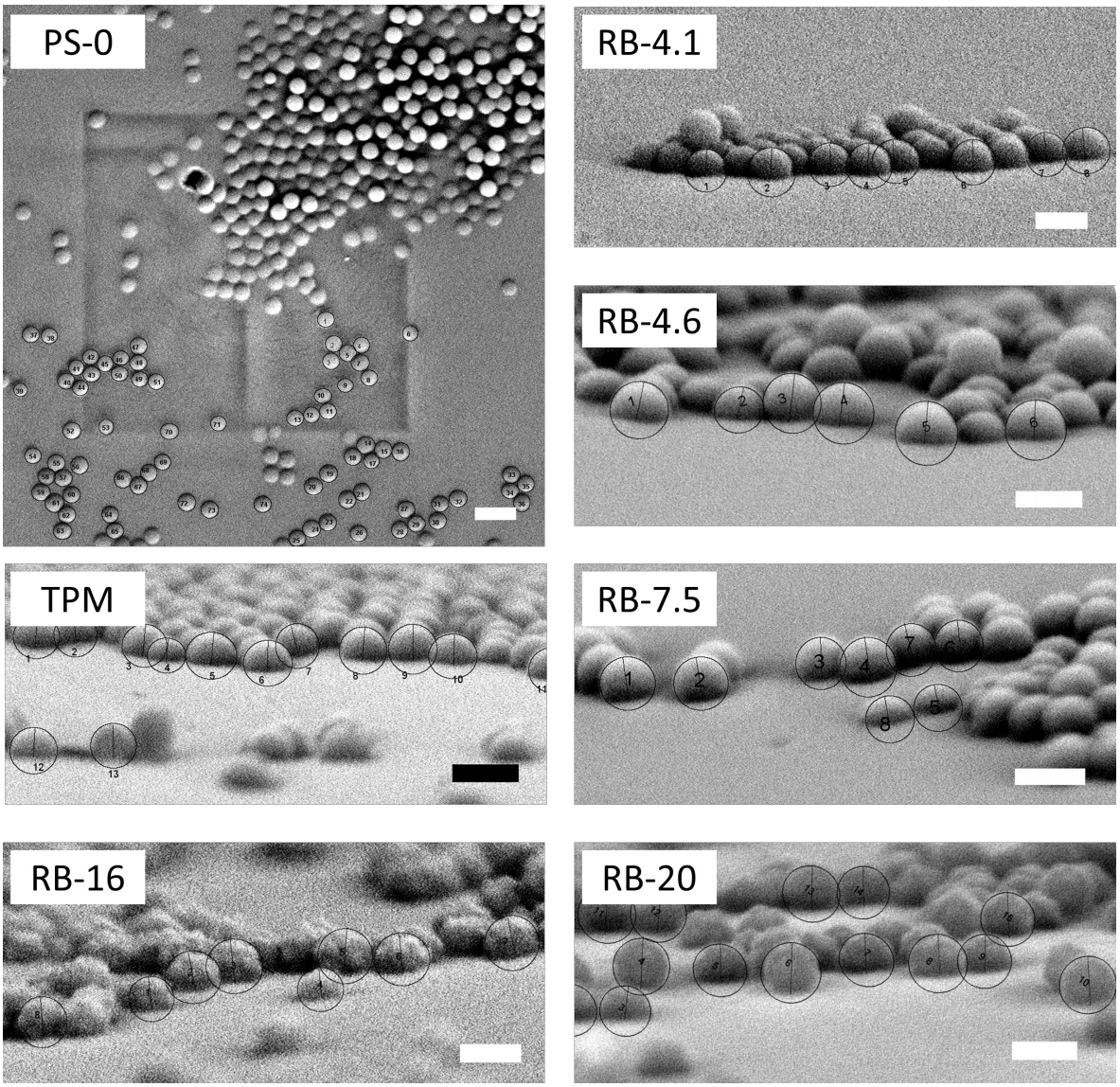

Figure A 5. Representative SEM images of interface replicas with PS, TPM and the raspberry-like particles. Scalebars: PS-0: 2 µm, other scalebars: 1 µm.

Contact angles of PS-0 were determined from top views of the interface. A top view image looks through the water phase on the oil phase (which is replaced by UV glue). In this configuration, the largest portion of a hydrophobic particle is immersed in the UV glue. Then, by comparing the particle radius at the interface with the actual particle radius independently obtained, the contact angle of the particle at the interface can be extracted according to the following relation (which is visualized in Figure A 6):

$$\theta = \theta_w = \sin^{-1}\left(\frac{S}{R}\right) \tag{12}$$

where S is the radius at the interface determined from the SEM image of the replica and R is the average particle radius as given in section 4.1.1.

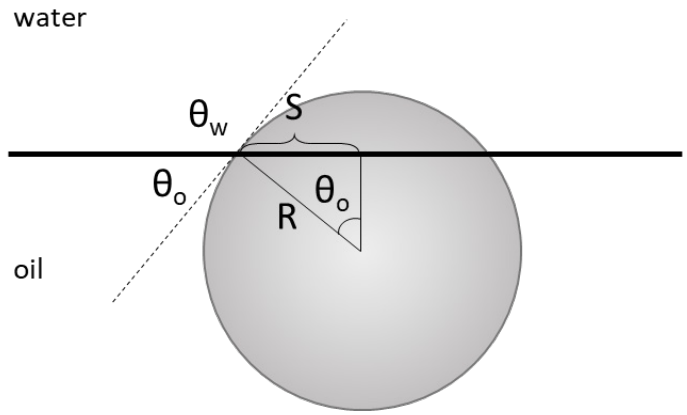

Figure A 6. The contact angle of a hydrophobic particle on the interface can be calculated from a top view SEM image by measuring the radius on the interface S and using the illustrated geometry.

Contact angles of the hydrophilic particles were determined from a cross-section of the interface. By measuring the height of the spherical cap H and the particle radius r on the SEM images of the interface replicas (see Figure A 7), the contact angle can be found using the following relation:

$$\theta = \cos^{-1}\left(\frac{|H - r|}{r}\right) \tag{13}$$

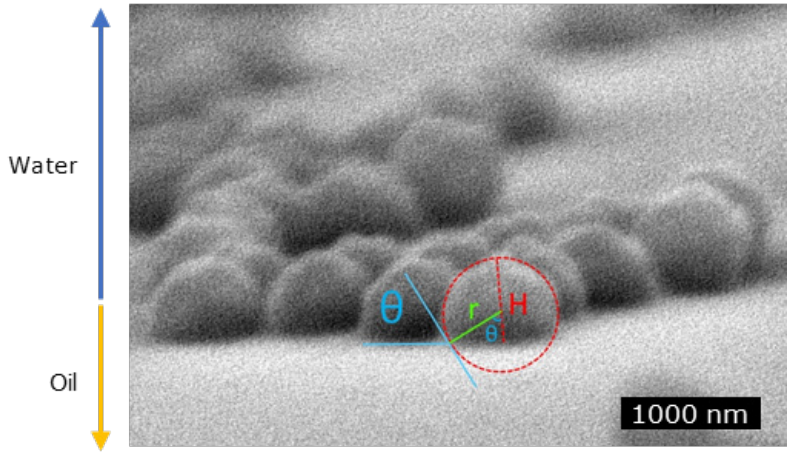

Figure A 7. Cross-section of an interface replica. The contact angle can be calculated from the measured cap height H and particle radius r.

APPENDIX E. ZETA POTENTIAL DISTRIBUTIONS PS CORES

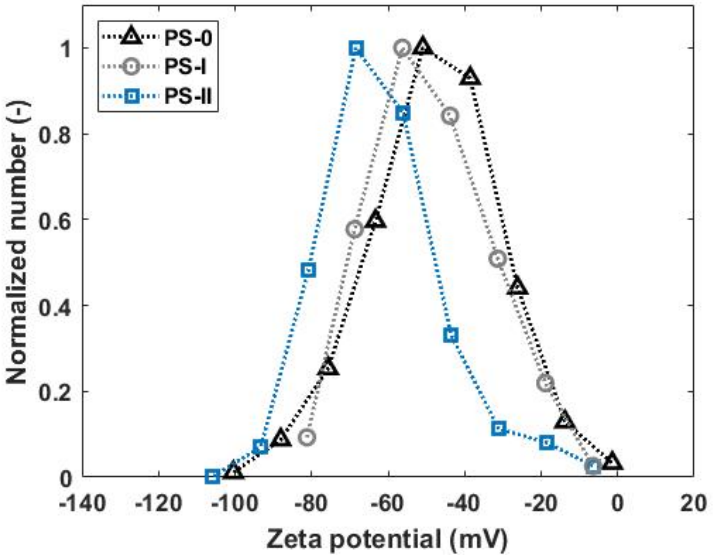

Figure A 8. Zeta potential distributions of the PS cores used for the patchy rough colloid synthesis.

APPENDIX F. EFFECT OF BODIPY ON INTERFACIAL TENSIONS AND EMULSIFICATION

Interfacial tensions of water and n-decane were measured at different concentration of BODIPY 493/503 to evaluate the effect of the BODIPY addition. At the same conditions, emulsions of the two phases in the absence of particles were prepared. The reason for measuring the interfacial tensions is that BODIPY can act as a surfactant, and the creation of surfactant emulsions relies on the lowering of the interfacial tension upon adsorption of surface active molecules.[54] Figure A 9 shows the slight decrease in interfacial tension with increasing concentration of BOPIDY in n-decane.

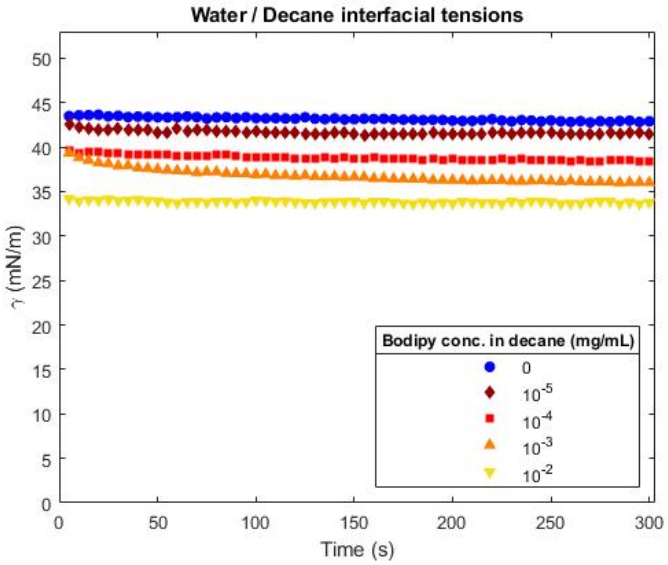

Figure A 9. Water / n-decane interfacial tensions (γ) at different concentrations of BODIPY in n-decane. Interfacial tensions were measured with a dataphysics OCA15plus Contact angle system by creating a water pendant drop[84] from a syringe with a dataphysics SNP-D 165/135 needle in a BODIPY/n-decane phase in an optical cuvette (Hellma 100-05).

Although the lowering of the water-decane interfacial tensions shows that BODIPY adsorbs on the interface, the used BODIPY concentrations do not produce significant emulsions (only some tiny white flakes are observed after 'emulsification', see Figure A 10). Therefore, it is not expected that the addition of BODIPY to the emulsion formulations containing particles will affect the emulsification. Still, to avoid any unexpected interference with the emulsification, the emulsions were prepared with the lowest possible concentration of BODIPY.

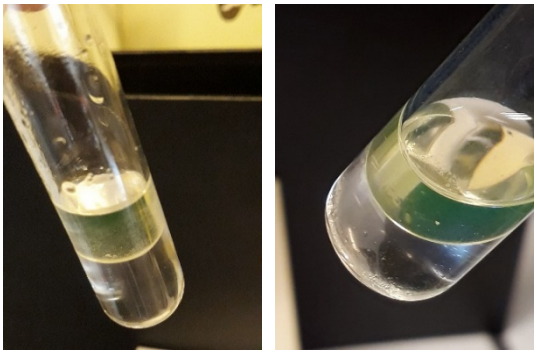

Figure A 10. 'Emulsification' of 10^{-3} (left) and 10^{-2} (right) mg/mL BODIPY in n-decane with water.

APPENDIX G. EMULSIFICATION CHALLENGES USING RB-20

It was noted that RB-20 particles usually do not form emulsions with droplets finely dispersed in the continuous phase, or even only form clumps of emulsion that stick to the tube walls and are easily destroyed by gentle handshaking. To a lesser extent, such limited emulsification was also sometimes observed for RB-16. Figure A 11 shows typical bright field microscopy images of emulsions with RB-20. The non-continuous structure of the emulsions is also visible in the macroscopic photograph in Figure A 11. Clusters of droplets, sometimes encapsulated by a film, cannot be separated without destroying the emulsion. A cause for this might be limited adsorption of the particles on the oil-water interface and extensive particle bridging.

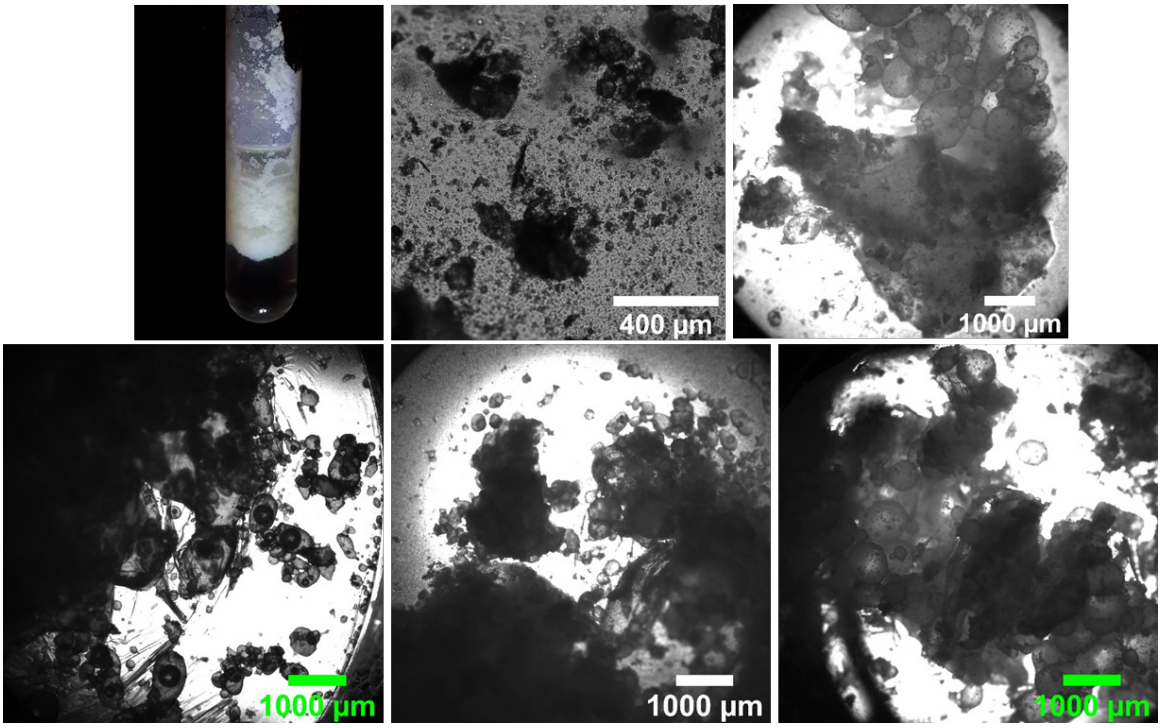

Figure A 11. Typical images of emulsions with RB-20 particles. Instead of finely dispersed droplets, clumps of droplets in various morphologies are present.

The adsorption of particles on a droplet might be limited due to a too high surface charge of the particles or due to the presence of many surface active molecules in the particle suspensions. The adsorption of a highly charged particle might be hindered by electric-double layer repulsion between a particle and the oil-water interface, or by the repulsion between a particle in the water and its image charge (of the same sign) in the oil phase.[85] The presence of surfactants might impede the particle adsorption as well. To check whether these effects could play a role in the emulsification of the patchy rough particles, zeta potential and interfacial tension measurements were conducted. Figure A 12a shows that the roughest particles have the smallest zeta potentials, thus are least charged. Increased repulsion between the particles and the interface or their image charge is therefore unlikely to be the cause for the scarce emulsification efficiency. Figure A 12b does not show any correlation between the suspensions of rough particles and the interfacial tensions of suspension/n-decane interfaces. Therefore, the presence of surface active species hindering the adsorption of the colloids can also be rejected as cause for limited emulsification with RB-20. Consequently, the roughness of the particles could cause the limited emulsification. Reduced Pickering emulsification stability for particles with a too high degree of roughness has been reported,[40] and was justified by a wetting transition from the Wenzel regime for particles of lower roughness to the Cassie-Baxter regime for particles of higher roughness (see section 2.2).

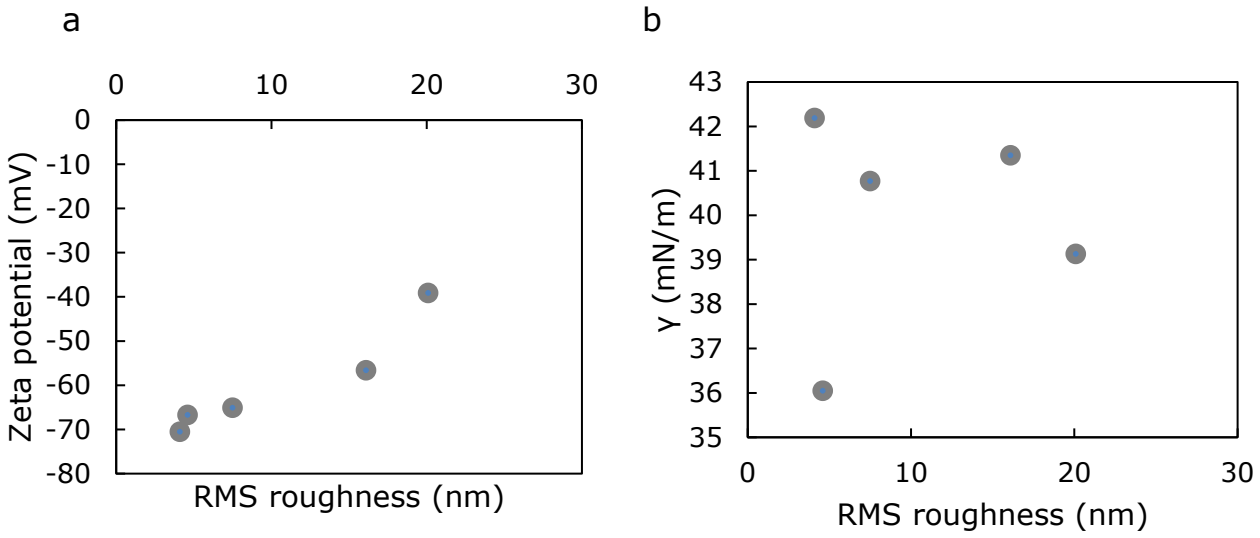

Figure A 12. (a) Zeta potentials of patchy rough particles. (b) Interfacial tensions of particle suspensions / n-decane interfaces.

Zeta potential measurements of ~0.03 wt% particle suspensions in 10mM KCl were conducted with a Malvern Zetasizer Nano ZS. Interfacial tensions were measured with the same system as described in the caption of Figure A 9 in Appendix F.

APPENDIX H. EMULSION PHASE INVERSION PER PARTICLE TYPE

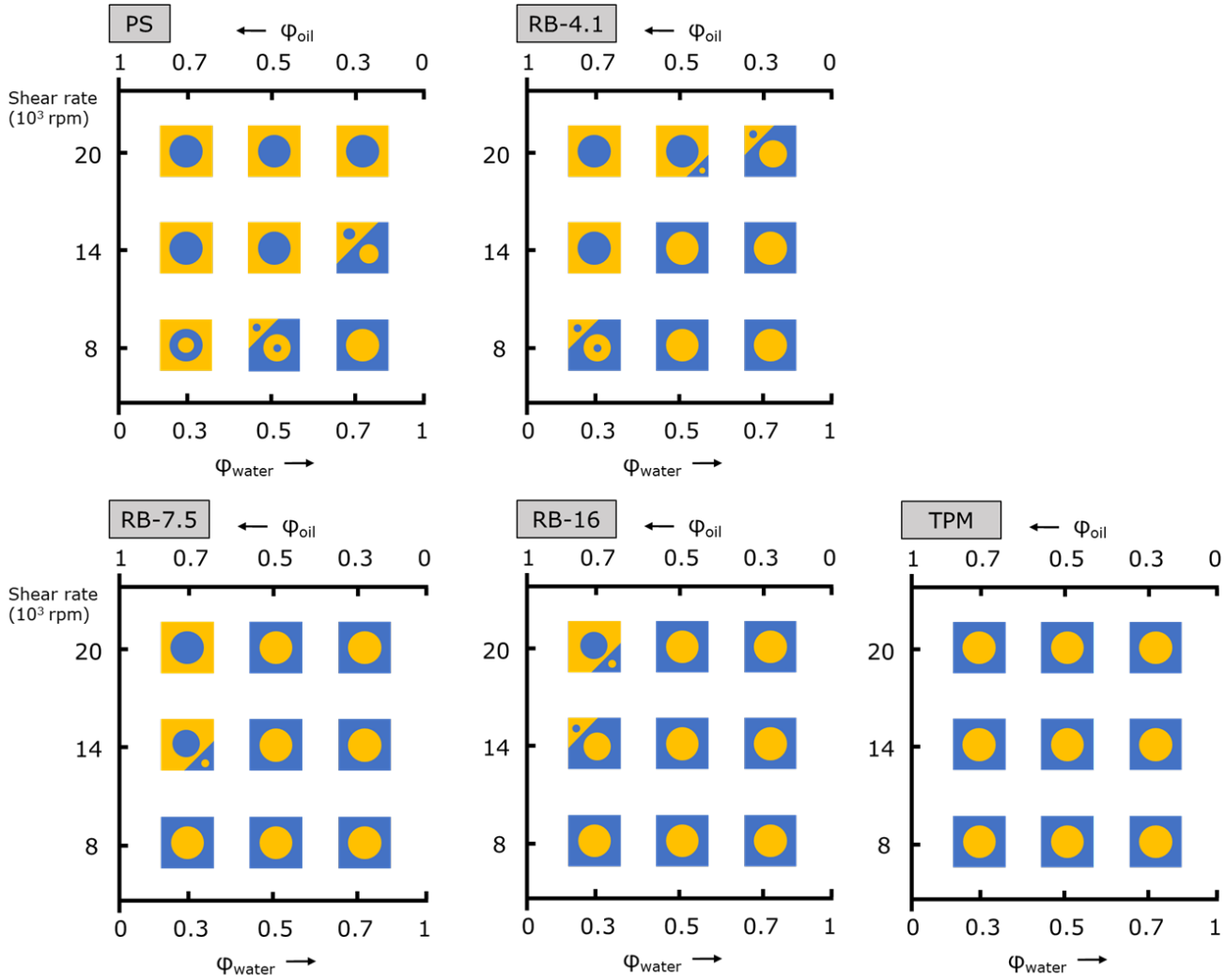

Figure A 13. Emulsion phase inversion diagrams per particle type. Increasing the water content (φ_{water}) in emulsions can result in catastrophic phase inversion. Mechanical phase inversion can occur with increasing emulsification shear rate. No phase inversion is observed for TPM for the probed conditions.

APPENDIX I. IMAGES OF EMULSIONS

In Figure A 14 - Figure A 18, images of all emulsions supporting the results in Figure A 13 are presented. Images are grouped per particle type.

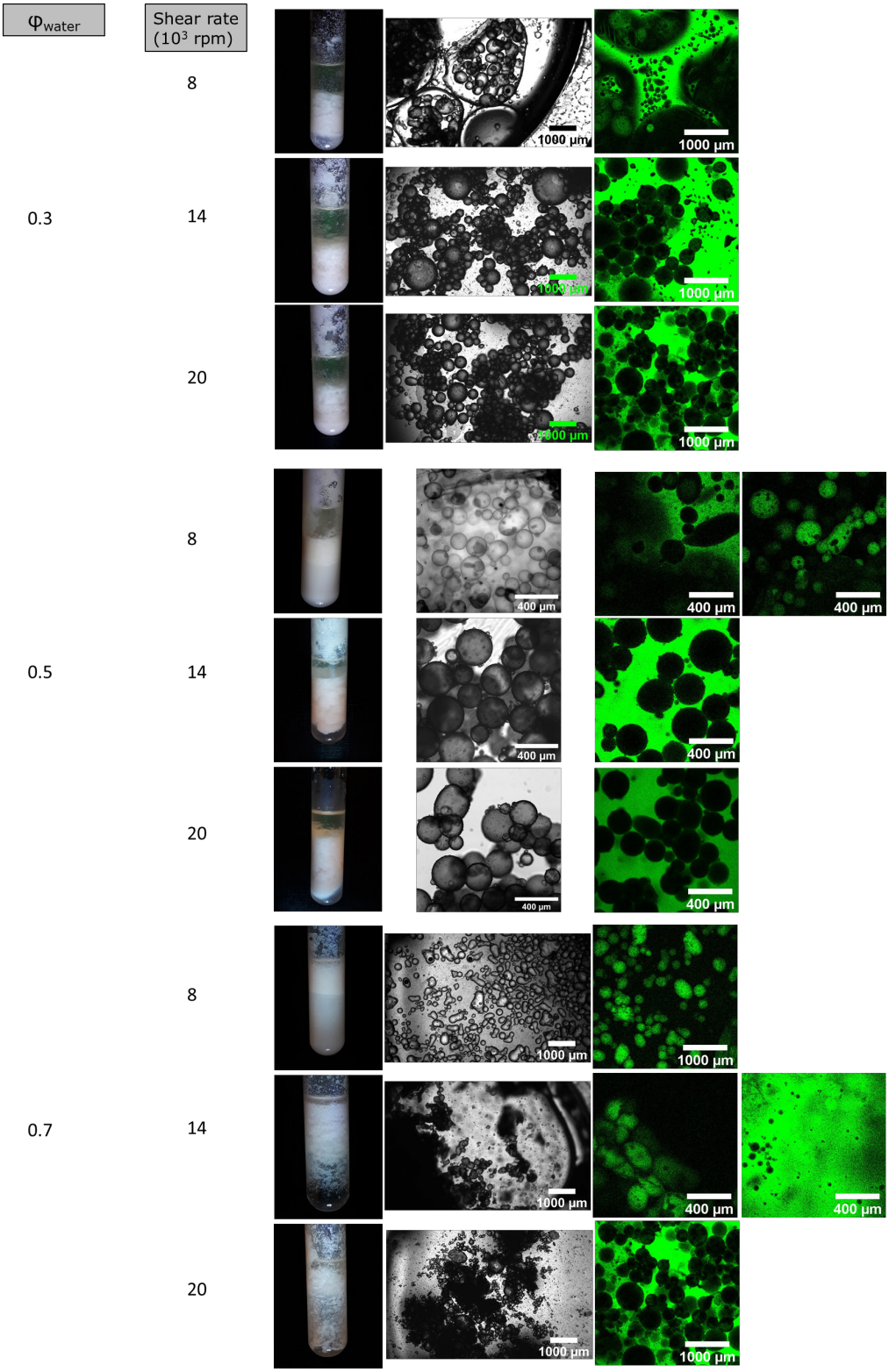

Figure A 14. Images of emulsions with PS. From the left to the right column: macroscopic, bright field optical microscopy and confocal fluorescence microscopy images. The confocal fluoresence microscopy images show whether the emulsions are o/w or w/o type by addition of BODIPY 493/503 to the n-decane oil phase.

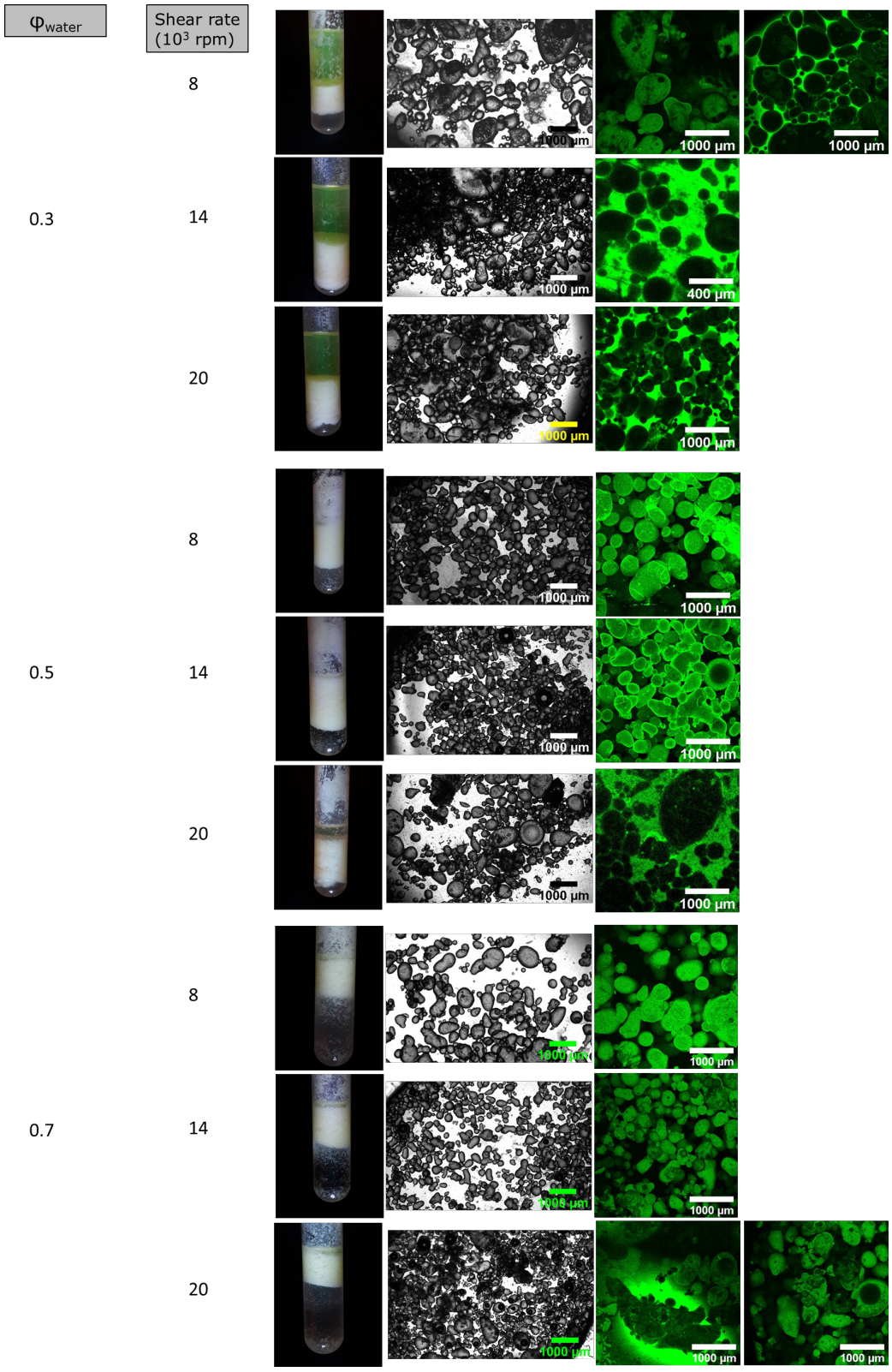

Figure A 15. Images of emulsions with RB-4.1. From the left to the right column: macroscopic, bright field optical microscopy and confocal fluorescence microscopy images. The confocal fluoresence microscopy images show whether the emulsions are o/w or w/o type by addition of BODIPY 493/503 to the n-decane oil phase.

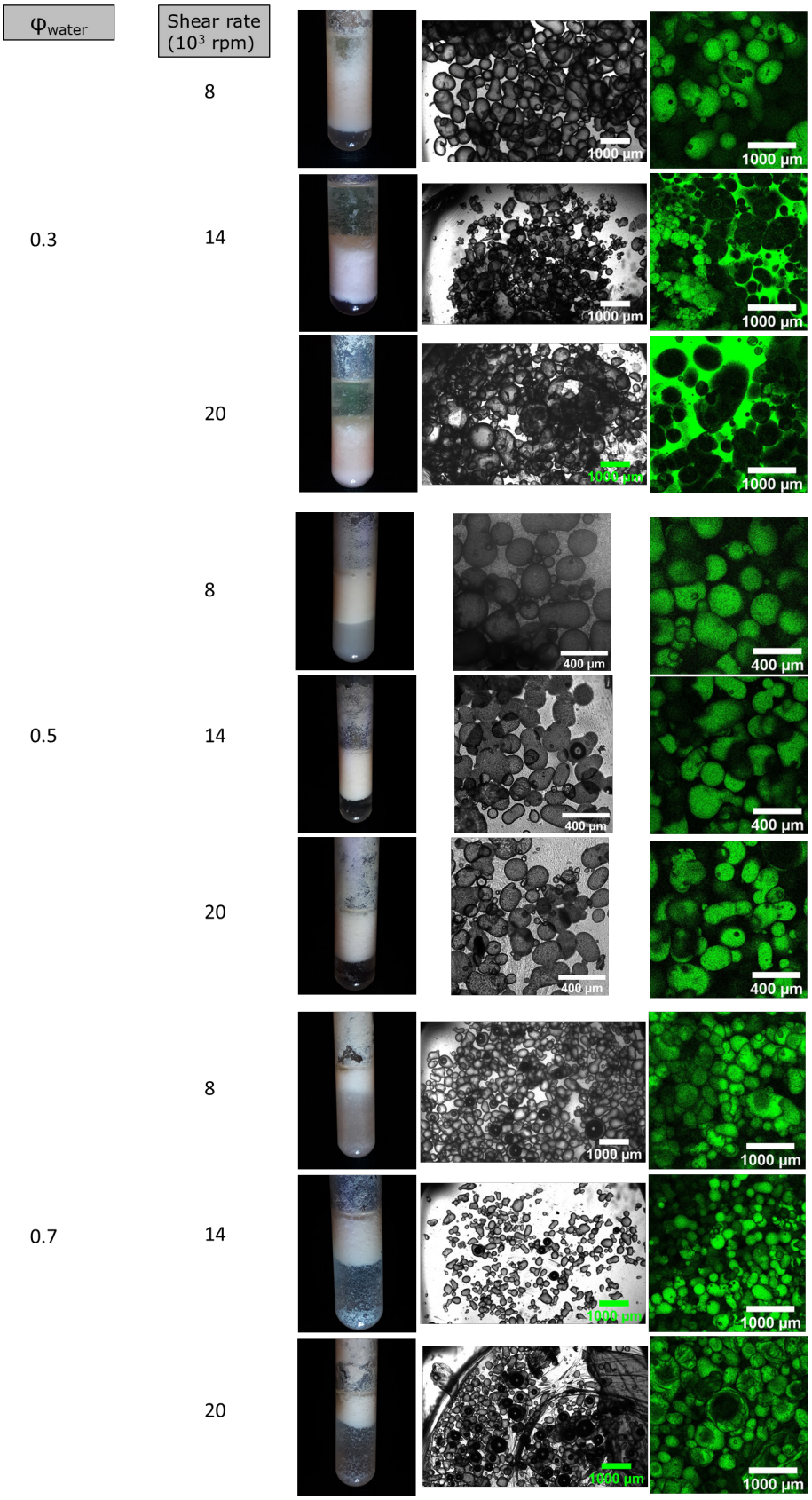

Figure A 16. Images of emulsions with RB-7.5. From the left to the right column: macroscopic, bright field optical microscopy and confocal fluorescence microscopy images. The confocal fluoresence microscopy images show whether the emulsions are o/w or w/o type by addition of BODIPY 493/503 to the n-decane oil phase.

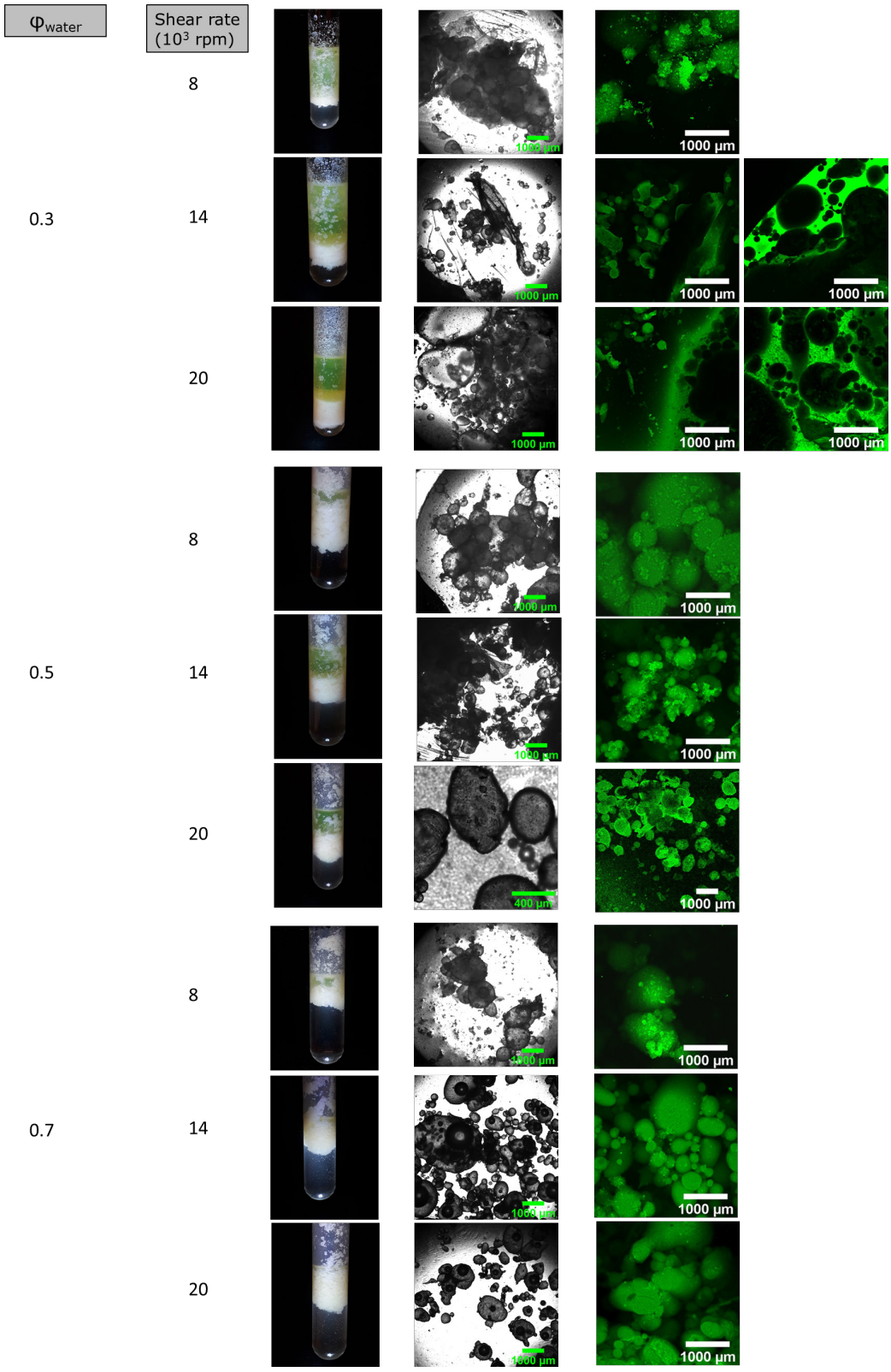

Figure A 17. Images of emulsions with RB-16. From the left to the right column: macroscopic, bright field optical microscopy and confocal fluorescence microscopy images. The confocal fluoresence microscopy images show whether the emulsions are o/w or w/o type by addition of BODIPY 493/503 to the n-decane oil phase.

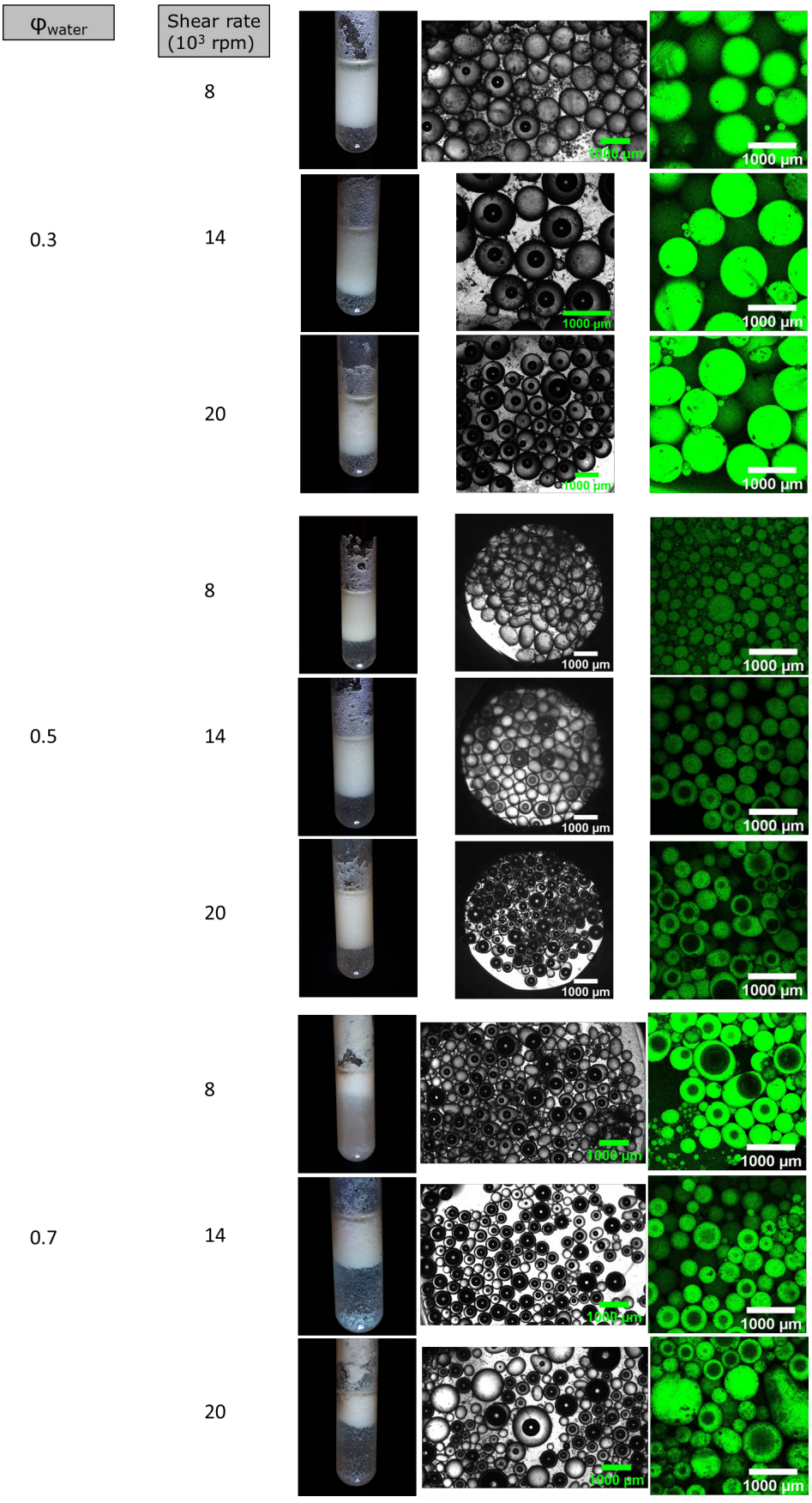

Figure A 18. Images of emulsions with TPM. From the left to the right column: macroscopic, bright field optical microscopy and confocal fluorescence microscopy images. The confocal fluoresence microscopy images show whether the emulsions are o/w or w/o type by addition of BODIPY 493/503 to the n-decane oil phase.